Structural Assessment of the Guastavino Masonry Dome of the Cathedral of Saint John the Divine

by

Hussam Dugum

Bachelor of Engineering in Civil Engineering and Applied Mechanics

McGill University, Montreal, 2012

Submitted to the Department of Civil and Environmental Engineering

in Partial Fulfillment of the Requirements for the Degree of

Master of Engineering in Civil and Environmental Engineering

at the

Massachusetts Institute of Technology

June 2013

Signature of the Author:

Department of Civil and Environmental Engineering

May 10, 2013

Certified by:

John A. Ochsendorf

Professor of Building Technology and Civil and Environmental Engineering

Thesis Supervisor

Accepted by:

Heidi M. Nepf

Chair, Departmental Committee for Graduate Students

Structural Assessment of the Guastavino Masonry Dome of the Cathedral of Saint John the Divine

by

Hussam Dugum

Submitted to the Department of Civil and Environmental Engineering
on May 10, 2013 in Partial Fulfillment of the Requirements for the Degree of
Master of Engineering in Civil and Environmental Engineering

Abstract

Historic masonry structures have survived many centuries so far, yet there is a need to better understand their history and structural safety. This thesis applies structural analysis techniques to assess the Guastavino masonry dome of the Cathedral of Saint John the Divine. This dome is incredibly thin with a L/t ratio of 200. Thus, it is important to assess this dome and its supporting arches, and confirm they are within adequate safety limits.

This thesis gives an overview of the basic principles of masonry structural analysis methods, including equilibrium and elastic methods. Equilibrium methods are well suited to assess masonry structures as their stability is typically a matter of geometry and equilibrium rather than material strength. Using membrane theory and graphical analysis equilibrium methods, a complete analysis of the masonry dome and its supporting arches under symmetric and non-symmetric loading was performed. The arches supporting the dome carry the orthogonal thrust coming from the dome to the main piers. This thesis presents a strategy on how to evaluate the flow of forces for such a system, based on the fundamental principles of equilibrium methods. The analysis demonstrates the safety of the dome of the cathedral under gravitational loading and determines that the steel reinforcing in the dome is unnecessary for the safety of the dome.

Thesis Supervisor: John A. Ochsendorf
Title: Professor of Building Technology and Civil and Environmental Engineering

Acknowledgements

I would like to express my deepest gratitude to all those who provided contribution and support throughout the development of this thesis. First, I would like to thank my advisor, Professor John Ochsendorf, for inspiring my research interest in the analysis of masonry structures. I am particularly grateful for his insightful feedback, and for all the great opportunities he has given me. He has taught me the value of perseverance and independent thinking, and for that I am very thankful. I want to express many thanks to the PhD students Rory Clune and Caitlin Mueller for their continuous input and support throughout the development of this thesis. I also want to thank all my JAO-MEng research colleagues, namely Virginie Arnaud, Trevor Bertin, Mayce El Mostafa, Romain Mesnil, and Emidio Piermarini. The weekly thesis seminars along these research colleagues provided an excellent opportunity to discuss and learn about our different thesis topics, provide valuable feedback to each other, and collectively, progress with our theses.

I want to thank Ms. Janet Parks and the rest of the staff at the Department of Drawings & Archives of Avery Library, for helping me find and use all the Guastavino original drawings of the Cathedral of Saint John the Divine. I also want to thank Mr. Wayne Kempton at the Archives Department of the Episcopal Diocese of New York, for providing me priceless images of the cathedral during construction and after.

I want to thank my brother and parents, who have provided me with unconditional trust and support throughout my whole life. Thank you for teaching me the value of dreaming big, hard work, patience, and perseverance, for without that, nothing I have achieved would have been possible.

Last but not the least, I would like to thank the MEng Class of 2013. It had been a great experience to work with you days and nights throughout last year. I have learned a lot from every one of you, and for that I am extremely grateful.

Contents

List of Figures

List of Tables

1 Introduction

1.1 Motivation

Masonry buildings are considered to be the backbone of structural engineering as they have been built for thousands of years so far. Masonry have been used as a construction material in many architectural eras, including Greek, Roman, Byzantine, Romanesque, and Gothic. Most masonry structures have resisted many natural events over the years of their existence. These events include earthquakes, differential settlements, and shifts of foundations. However, the longevity of these structures implies that they have been designed using efficient analysis methods and construction techniques.

Architects and builders who designed historic masonry structures lacked the modern analysis software tools and the endless structural design resources that are present now for structural engineers to refer to. Yet, these builders had an intuitive understanding of equilibrium and were able to design magnificent structures which lasted for many years. As a structural engineer, it is important to understand how these builders designed such structures in the past, and what were the structural analysis and construction methods that they used. Such a knowledge establishes an instinctive understanding of structural behaviour, and how the analysis and design methods may evolve in the future.

This thesis presents a complete structural assessment of the masonry dome of the Cathedral of Saint John the Divine. The dome was designed and constructed by the great architects Rafael Guastavino Sr. (*1842-1908*), and his son, also Rafael (*1872-1950*), and is an exceptional combination of intricate structural analysis application and ingenious construction techniques.

1.2 The Cathedral of Saint John the Divine

The Cathedral of Saint John the Divine, shown in Figure 1.1, is affiliated with the Episcopal Church and is located in Manhattan, New York City. The cathedral competes with the Liverpool Anglican Cathedral for the title of the largest cathedral in the world. The floor area inside the church covers 121,000 ft^2, spanning a length of 601 *ft* and height of 232 *ft*, and the inside height of the nave is 124 *ft*. [1] After an open competition to design the cathedral in 1891, the design by the New York firm Heins and LaFarge was the winner, and so took the lead on the design of the cathedral. The cornerstone of the cathedral was laid in 1892, and the central nave was completed in 1909. [1]

The cathedral was originally designed with a tall spire to cap the four great crossing arches. In 1909, and after the completion of these arches, the construction slowed down and the costs were unpredictably increasing. As a result, the tower could not be constructed at the expected date. By then, Guastavino Jr. came up with an excellent alternative instead of the spiral tower. He suggested to build a masonry dome instead of the tall spire. Guastavino Jr. said that this alternative could be built without the need of falsework, and so construction would be faster and cheaper. He justified his suggestion by the fact that domes can be built without falsework if they are constructed in a series of concentric rings. This type of

construction is self-supporting, and so would prevent the dome from falling inward during construction. [2]

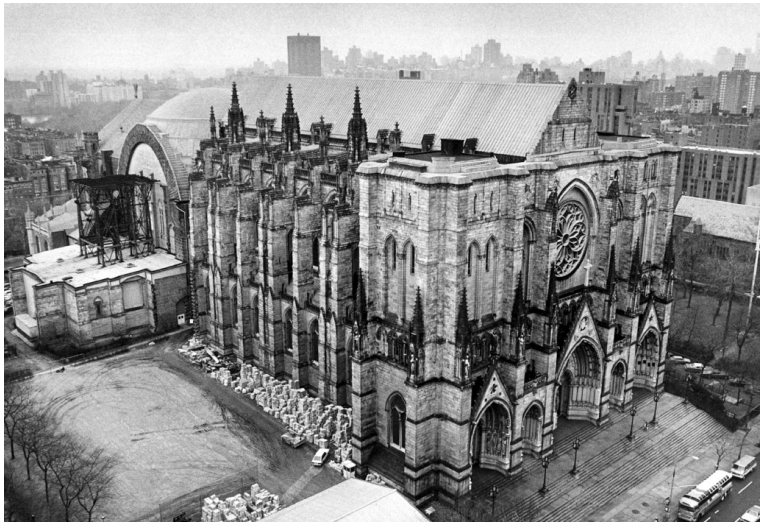

Figure 1.1: The Cathedral of Saint John the Divine [3]

Guastavino Jr. submitted his proposal to the architects and was accepted to proceed with. In 1909, Guastavino Company completed the construction of the dome over a span of 15 weeks only, with a total cost of $10,300. [2] The construction time was relatively short because of the absence of scaffolding support or falsework. As a result, Guastavino Jr. succeeded in constructing one of the largest masonry domes in history at a much lower cost than any other dome of its size.

1.3 Construction of the great arches and the dome

1.3.1 The great arches

Some of the most interesting structural features of the cathedral are the four supporting arches of the dome, or the "four great arches", which were built by others prior to the Guastavino dome. Each arch has a cross section of 12x12 ft^2, with a clear span of 85 *ft* and a rise of 58 *ft*. The baseline of the arches is 74 *ft* above the ground level. The four arches are supported by four main piers, each having a cross section of 21x21 ft^2. There are two flying buttresses bearing against each of the four main piers, and each has a cross section of 12x13 ft^2, and have a radius on the intrados of 43 *ft*. The span is 21 *ft*, and they rest on the piers 44 *ft* above the ground level. [4] The great arches, the main piers, and the flying buttresses are constructed of granite masonry, and are partially concealed by exterior architectural features. Figure 1.2 shows one of the great arches and its corresponding piers during construction.

Four centering trusses, spaced 3 *ft* apart, were used as formwork for each of the great arches, as shown in Figure 1.3. These trusses were built on the ground and, generally, took two days to raise them from the ground to their position and place the transverse bracing in between. The same length of time was also required to remove them after the arches had been completed. Only one set of centering was used for the four arches, work being carried on with only one arch at a time. The complete centering for one arch,

including the four trusses and the transverse bracing, contained a total of 23,500 ft of lumber and 8,500 lb of bolts and washers. [4]

Figure 1.2: Construction of one of the great arches and its corresponding piers [3]

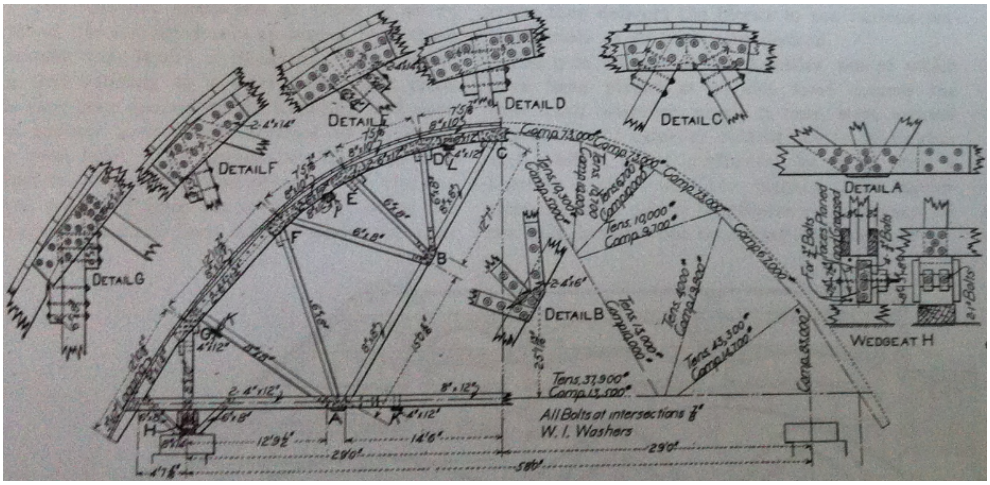

Figure 1.3: Detailing of the centering truss [4]

The granite materials were brought from Mount Waldo in Maine, and the arch voussoirs were cut in sections of 4x6x2 ft^3. These voussoirs were jacked up from the ground into position using derricks, and the arches were constructed one layer at a time, filled with concrete in between. The construction of each of the arches took an average of three months, with about eight working hours a day. [4]

1.3.2 The dome

The spherical dome, which is the complete dome above the arches, has a radius of 66 *ft* and a diameter of 98 *ft* at the base, where it rests on the pendentives, which are spherical triangles of the same radius, as shown in Figure 1.4. The dome is being supported by the four great arches and by the pendentives. The latter being continuous with the dome and virtually forming extensions of it, increasing its maximum diameter to 132 *ft*, and the rise of the center to 66 *ft* above the baseline of the arches, making the total height of the top of the dome 161 *ft* above the ground. [5]

Figure 1.4: The dome [3]

The pendentives, shown in Figure 1.5, have a uniform thickness of 9 courses, or about 12 *in*, of solid tiles and cement reinforced by four horizontal levels of steel ties embedded in cement to take up the hoop tensile stresses. Above the pendentives, the thickness of the dome decreases from 7.5 *in* at the base to 4 *in* at the crown, corresponding to thicknesses of 5,4 and 3 courses of tiles, and is reinforced with one horizontal level of steel ties at its base to take up the hoop tensile stresses during construction. The average dead load of the dome is 50 *psf*, which is considered extremely light for a masonry structure of such span, and the total weight was estimated at about 500,000 *lb*. [5]

Figure 1.5: Pendentives of the dome under construction [3]

All portions of the completed dome were at all times self-supporting during construction, and it was built entirely without falsework or centering. The tiles were constructed in a series of concentric rings, and circular templates, which carried loads, were used as guides in setting the tiles. In laying the tiles, the lower course was at first supported wholly by the adhesion of the plaster paris mortar on the edges of the tiles. This first course would harden rapidly to make it self-supporting and was strong enough to carry the succeeding courses until the portland cement mortar in between them hardened.

As the work advanced, exterior scaffolds were built up vertically above the side walk and the main arches, and the work was continued from them. As the work kept advancing, as shown in Figure 1.6, the angle kept increasing and the overhang became more and more apparent, and the surface was flat enough for the men to work directly on it. When it became apparent that the men were working on the very thin, overhanging dome at a great height above the ground, some of the workers became nervous, but the more experienced continued the work without difficulty, advancing and reaching over the edge of the last course to lay the next one without other support than the recently completed thin dome. No accidents occurred, and only one or two tiles, which probably were not held quite long enough in setting, fell to the floor below. [5]

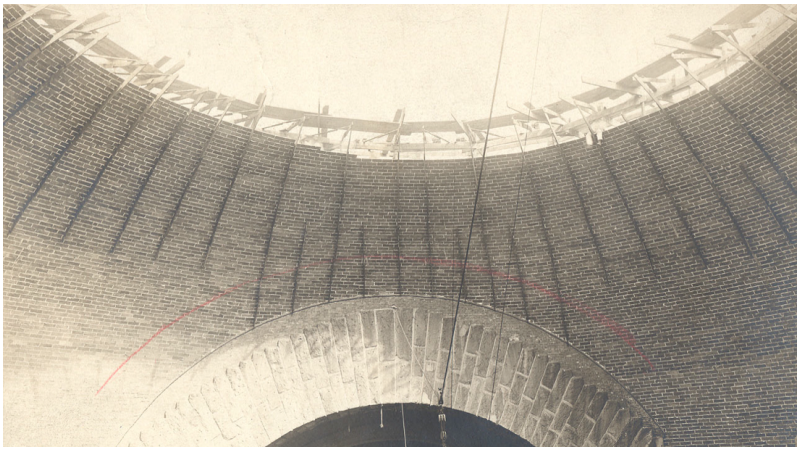

Figure 1.6: The dome under construction [3]

It is estimated that falsework and centering built up from the ground below in the usual manner, would have cost nearly $2,000. [5] This cost, together with the considerable cost of removing the falsework was avoided by the very courageous and ingenious Guastavino construction method.

1.4 The Guastavinos

Rafael Guastavino Sr. was born in 1842, in Valencia, into a large family of musical craftsmen. He played the violin as a teenager and was aspired to become a musician. His interest in architecture was sparked after he worked at his uncle's textile factory in Barcelona, where he gained an important insight into its design and operation. In 1861, he began his studies at the *Escola Especial de Mestres d'Obres*, or "Special School for Masters of Works", where he was taught by the best professors of that period. In 1872, Guastavino graduated from the school with the professional title of *mestre d'obres*, or "master of works". [2]

As an apprentice master builder, Guastavino gained familiarity with the construction techniques and materials used in the region. Guastavino had a special interest in tile vaulting and decided to focus his works using this construction material. Tile vaulting is a building system that was created in the Mediterranean Region in the fifteenth century. [2] This construction technique was very efficient in terms of economy of materials and its speed of construction. The tiles were typically 4 inches thick, but were fireproof and incredibly strong. Guastavino built many fascinating structures in and around the region. The most notable of these projects are the Batllo Factory in Barcelona, and La Massa Theater in Vilassar de Dalt. In 1881, Guastavino decided to leave Spain with his youngest son, also Rafael, for the United States, both are shown in Figure 1.7. The decision to emigrate was based on a combination of factors, but mostly because he saw a great business opportunity for tile vaulting in the growing american cities.

Figure 1.7: Rafael Guastavino Sr. (*1842-1908*) (left) and Rafael Guastavino Jr. (*1872-1950*) (right) (Guastavino/Collins Collection, Avery Library)

Upon arrival to the United States, Guastavino struggled in defining his new professional path because of the different American building practices. This was particularly difficult due to the increasing demand of higher building performance in terms of safety and fireproofing. His first major project in the United Sates was at the Boston Public Library, where he built his signature arched vaults. His successful collaboration with the firm of architects McKim, Mead and White in that project led to the many commissions over the few decades after.

The sublime techniques of Guastavino's work was performed on more than two hundred buildings in Manhattan, and in hundreds more across the United States, including the Grand Central Terminal, Carnegie Hall, Saint Paul's Chapel, Nebraska State Capitol, and the Cathedral of Saint John the Divine. Guastavino's unique vaulting techniques had been patented, and, together with his son, Guastavino held 24 different patents. [6]

In 1889, Guastavino Sr. established the Guastavino Fireproof Construction Company, and in 1900, started a factory in Woburn, Massachusetts, that produced the custom-made tiles needed for his designs. Guastavino Sr. died in 1908, and by then, the tile factory in Woburn had considerably expanded its design capabilities. From there, Guastavino Jr. took the lead of the business and ensured the continuous success and expansion of the company.

The demand for Guastavino vaulting began to decline in the 1930s. The tile processing became labor intensive and pricy, and the angular style of architecture was growing. And that style was better achieved using steel or reinforced concrete. Guastavino Jr. died in 1950, and the Guastavino Company operated for almost one more decade before it permanently closed in 1962, after 75 years of constructing some of the most fascinating American architecture.

1.5 Problem statement

This thesis aims to analyze the masonry dome of the Cathedral and its supporting arches, using equilibrium analysis methods. With the geometry of this dome and its extreme thinness, it is essential to asses the safety of the structure under various loading conditions. The key problems that will be addressed in this thesis are:

- Apply and compare the different equilibrium analysis methods in analyzing masonry structures
- Determine possible thrust lines for the dome under self-weight and under non-symmetric loading conditions, calculate the meridional and hoop forces within the dome, and confirm that the design criteria is based on equilibrium rather than strength
- Evaluate the necessity of the steel ties within the dome, and calculate the forces resisted by these tiles
- Determine possible thrust lines within the four great arches supporting the dome, and calculate their safety factor

The latter key problem has not been approached in previous studies. The supporting arches carry the orthogonal thrust coming from the dome towards the four main piers. This thesis provides a strategy on how to evaluate the thrust lines for such a structural system, based on the fundamental principles of equilibrium methods.

1.6 Outline of chapters

The introduction section defines the motivation and the main key problems that will be addressed in this thesis. The introduction includes a brief background of the cathedral, the design and construction process of the dome and its supporting arches, and a brief history about the builders of the dome.

The literature review section goes over the basic principles of structural analysis, and the analysis of masonry domes in specific. The section reviews and compares the various equilibrium and elastic analysis methods. A brief description of the Guastavino masonry tiles is given too.

The first section of the analysis presents an analysis on a generic masonry dome. This section explains the methodology of the analysis methods and presents their application and results on the generic masonry dome, after which they are being discussed.

The second section of the analysis presents the analysis on the masonry dome of the cathedral. The section

starts with an overview of the dome and its dimensions. From there, a complete analysis and discussion of the results are presented. The analysis includes the assessment of the dome under symmetric and non-symmetric loading, the assessment of steel ties within the dome, and finally the assessment of the arches supporting the dome.

The last section summarizes the main results of this thesis, and presents possible areas for future work.

2 Literature review

2.1 Basic principles of structural analysis

Masonry can be used as a structural material in various structural members, including arches, domes, vaults, buttresses, etc. Regardless, their basic structural behaviour and load transfer stem from the properties of masonry as a material. In general, any type of structure built from masonry or otherwise, must satisfy three main structural criteria in order to be safe and serviceable. These criteria are strength, stiffness, and stability. [7] Satisfying these criteria ensures that a structure is strong enough to carry its own weight plus any imposed loads. They also ensure that the structure is not going to deflect to the point where it becomes unsafe or not serviceable.

For unreinforced masonry structures, the stability and design of the structure is governed by the geometry of the structure rather than the material strength.The reason of that will become apparent throughout this thesis, and it is a fact that the actual stresses are lower than the material capacity in a typical masonry structure. For example, a typical masonry material such as sandstone may have a unit weight of 125 *pcf* and a crushing stress of 840,000 *pcf*. Dividing the crushing stress by the unit weight gives a value of around 6,700 *ft*. This means that a column of sandstone needs to be 6,700 *ft* to crush under its own weight. Obviously this is an unrealistic column height, and so masonry failure by insufficient strength does not usually occur. Also, one shall not worry about the stiffness of masonry structures. Masonry structural members are usually stocky, and so buckling or other deflection possibilities does not occur.

This leaves the third and last design criteria, that is stability, to be the most relevant for masonry structures. A simple illustration of the nature of the stability criteria is shown in Figure 2.1, the top block will remain in its position until the load P is large enough to cause the top block to fall of the edge. This illustration clearly shows that the stability of the top block is simply based on its geometry and self-weight, and the magnitude of load P. This system cannot be solved by linear elastic methods.

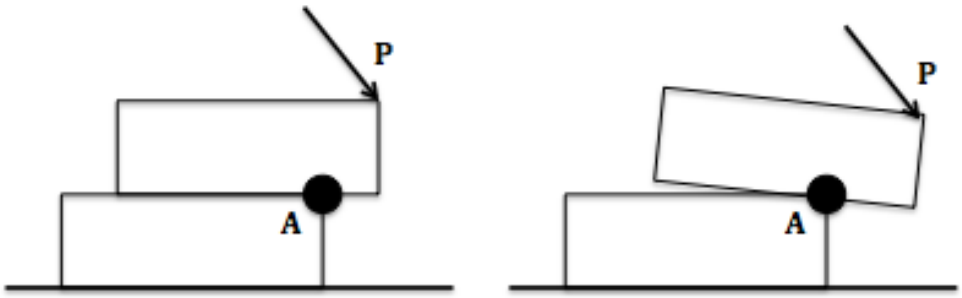

Figure 2.1: Example of stability analysis [8]

2.2 Equilibrium analysis of masonry structures

As was concluded in §2.1, the stability of masonry structures is governed primarily by their self-weight and geometry, and equilibrium analysis methods are necessary to analyze these type of parameters. The analysis of masonry structures is also based on these three fundamental assumptions: [7]

- Masonry has no tensile strength
- Masonry has infinite compressive strength
- Failure by sliding will not occur

The first assumption is conservative, because masonry itself has some tensile capacity. But the assumption is based on the fact that the mortar between masonry blocks is very week in tension, and collectively, the masonry structure would be pulled apart under any tensile forces. The second assumption is based on the fact that stresses in masonry stones are relatively small compared to the compressive strength of masonry, as was demonstrated in §2.1. However, one should keep in mind that localized crushing may take place, and so should be considered in design. As for the last assumption, it is considered that masonry blocks would not slide against each other, as there is sufficient friction between the blocks to prevent sliding.

Based on these assumptions, equilibrium and graphical analysis methods have been developed to determine the stability of masonry structures. All of the different methods are based on the fact that the self-weight of the structure, and any imposed loads, are carried as compressive forces through the structure in what are called as thrust lines. This means that for indeterminate masonry structures, there is more than one way to carry the load through the structure towards the base. In other words, they are infinitely many equilibrium configurations for indeterminate masonry structures. This principle was first formulated by Robert Hooke in a paper published in 1679. The principle says: *As hangs the flexible line, so but inverted will stand the rigid arch.* [7] This principle means that the shape of a chain hanging in pure tension under its own weight is exactly the same as the shape when it is flipped, but in this case it will behave as an arch under pure compression.

Under a specific loading condition, masonry structures have infinitely many thrust line configurations and load paths within the thickness of the arch. An arch will remain stable as long as the thrust line is maintained within the thickness of the structure from the crown and towards the base. The exact state of the stresses or the location of the thrust line is difficult to determine using the graphical analysis methods. That is why such structures are considered to be statically indeterminate with infinitely many load paths. This leads to the concept of safe theorem. [7] The theorem states that if at least one possible thrust line is determined within the thickness of an arch, it is correct to assume that the structure is stable and safe. Although this calculated thrust line may not be the actual thrust line where the loads are passing, but determining at least one possible thrust line ensures the stability of the structure.

The actual state of the thrust line of an arch may change due to multiple reasons. These include an addition of non-symmetric live, snow, or wind loads, or maybe foundation settlements, or natural events such as earthquakes. Regardless, the thrust line of the structure will change, and so it is important to assess

the stability of the structures in case of occurrence of such events, but first, one must understand the stability limits and collapse mechanisms of such structures.

If the thrust line approaches the intrados or extrados at any point along the structure, a "hinge" will form at that point. This hinge causes the thrust line and the forces in the structure to pass through it, and so rotation occurs. If enough hinges are formed, a possible collapse mechanism will form. [7] As hinges form, cracking would appear opposite to these hinges either at the intrados or extrados of the structure. However, the appearance of such cracking is not a sign of imminent collapse of the structure. Arches with up to three hinges are stable and safe. However, such cracking may cause the masonry blocks near the cracking location to fall and so affecting the serviceability of the structure.

If more than three hinges are developed for an arch, a collapse mechanism will occur and the arch will fail. The thrust lines will pass through the formed hinges, and an arch with three hinges is statically determinate. So the actual thrust state can be determined, and the stability limits, or the horizontal component of the support reactions at the base, can be calculated. Figure 2.2 shows a stable arch and the formed hinges under maximum and minimum thrust states. As long as the horizontal thrust is between H_{min} and H_{max}, the thrust line will be maintained within the thickness of the arch and it will remain stable. Out of this range, a collapse mechanism will occur and the structure will fail.

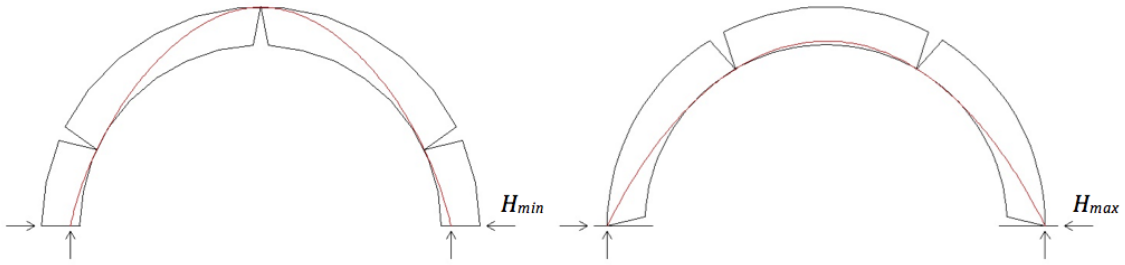

Figure 2.2: A stable arch under minimum thrust state (left), and under maximum thrust state (right)

2.3 Structural analysis methods of masonry domes

The same basic principles and assumptions of arch analysis are applicable to the analysis of masonry domes. Masonry blocks of the dome are assumed to have infinite compressive strength, zero tensile strength, and no failure by sliding. With that, the analysis methods of an arch can be expanded with a few more details and be applied to the analysis of masonry domes. Different analysis methods have been developed for the analysis of masonry domes, and can generally be classified as either equilibrium methods or elastic methods. Equilibrium methods determine the stability of the dome based on its geometry and self-weight. The equilibrium methods that will be used in this thesis are membrane analysis and graphical analysis methods. The elastic methods determine the forces based on the material strength and elasticity, and these methods are sensitive to the boundary conditions of the structure.

Both types of analysis methods evaluate the primary internal forces within the masonry dome, as shown in

Figure 2.3. The meridional forces transfer gravity loads from the crown towards the base of the dome. The hoop forces act in the latitudinal direction as concentric rings. The self-weight of the dome and any imposed loads are carried through these internal forces, and the distribution of forces within these orthogonal paths causes the dome to remain in equilibrium. The following sections will go over each of the analysis methods in more details.

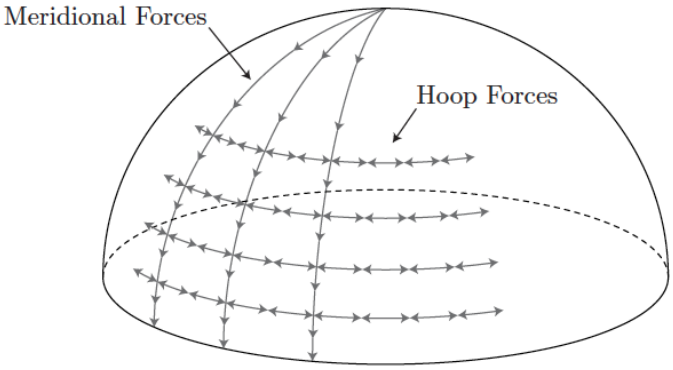

Figure 2.3: Primary internal forces in a masonry dome [9]

2.3.1 Membrane analysis

In membrane analysis, the masonry dome is assumed to be infinitely thin and acting as a shell surface at the centerline within the thickness of the dome. The surface would have no stiffness in bending, and so the forces carried in the shell are purely in tension or compression. In this analysis method, both meridional and hoop stresses are being calculated. [7]

The surface is analyzed as small shell elements, and stresses at equilibrium state are calculated accordingly. From Figure 2.4, θ is the longitudinal coordinate of an element with respect to a reference point, and ϕ is the latitudinal coordinate of an element, where $\phi = 0$ at the crown of the dome. Meridional stresses, N_ϕ, are the stresses along the meridians of the shell. Hoop stresses, N_θ, are orthogonal to the meridional stresses and occur at the same latitudinal level within the dome. If the radius of the dome is denoted as a and the weight per unit area is denoted as w, where w is the product of the density of the dome by the thickness of the dome, then N_ϕ and N_θ are calculated to be: [7]

$$N_\phi = -\frac{wa}{1+\cos(\phi)} \tag{2.1}$$

$$N_\theta = wa\,(\frac{1}{1+\cos(\phi)} - \cos(\phi)) \tag{2.2}$$

Note that the units N_ϕ and N_θ are *lb/ft*. The stress (*psf*) is obtained by dividing these terms by the density of the element, and the force (*lb*) is obtained by multiplying these terms by the width of the element.

The Meridional stresses are zero at the crown of the dome and increase in compression towards the base. This is because the cumulative gravity loads keeps increasing towards the base up to a maximum value of wa at $\phi = 90°$. Hoop stresses are under maximum compression at the crown with a value of $-wa/2$. And decrease in compression towards the base until it reaches the neutral axis, and then increase in tension up to a maximum value of wa at $\phi = 90°$. With the membrane analysis method, the neutral axis where hoop forces turn from compression to tension is always at $\phi = 51.82°$. The derivation of this angle is presented in Appendix A.

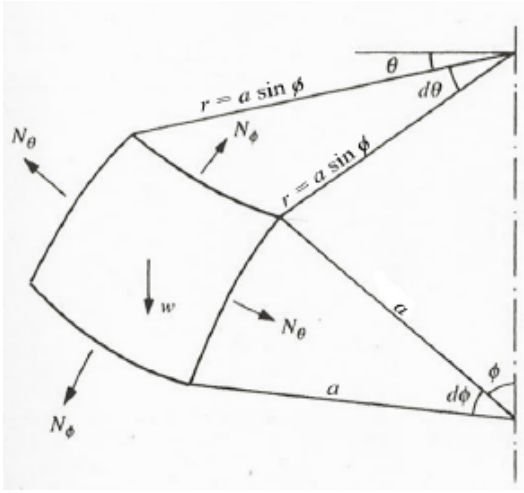

Figure 2.4: Equilibrium of a small element of a shell [10]

It was mentioned earlier that one of the basic assumptions about masonry is that it has no tensile capacity. With this assumption, masonry domes are bound to crack due the tensile hoop stresses towards the base of the dome because of the tensile hoop stresses. The nature of the cracking is illustrated in Figure 2.5, and this type of cracking is the case of many historic masonry domes. However, such cracking does not mean that the dome is unstable. Based on the safe theorem, if a possible thrust line is determined for a dome, even after cracking, then the dome should remain safe and stable. This makes sense because after cracking, the segmented dome sections will behave as independent arches, and will carry the imposed loads accordingly.

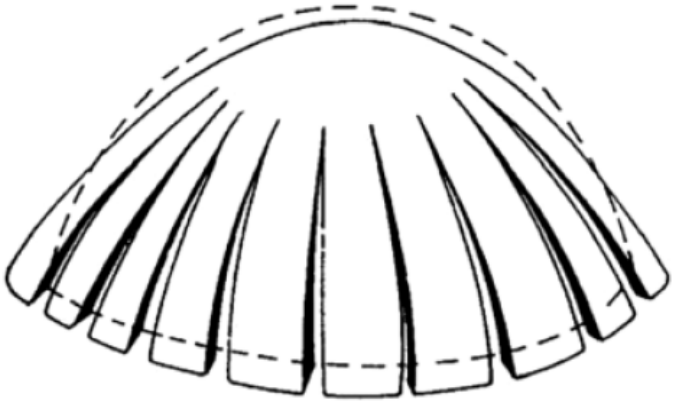

Figure 2.5: Greatly exaggerated illustration of a cracked dome [7]

2.3.2 Graphical analysis

Graphical analysis methods are equilibrium methods that determines the meridional and the hoop forces for a given masonry dome. The graphical analysis method that will be used in this thesis is the one developed by Wolfe in 1921. [11] The method determines the hoop and meridional forces in one slice of a dome, called lune. This lune has a certain width, defined by the angle θ, and this lune will be further divided into sections along its length. The method calculates the meridional and the hoop forces for each section along the length of the lune. The meridional forces are restrained to be in the mid-surface of the dome thickness in each section of the lune. And the magnitude of the hoop forces are determined in such a way to satisfy this restraint. Wolfe proposed two ways to approach his graphical analysis method. The first one assumes there is a tensile capacity for the dome, and the other one assumes there is no tensile capacity for the dome. Figure 2.6 shows both of the graphical analysis methods. Fig. 500 and Fig. 501 on the left demonstrate the method for a dome with tensile capacity, and Fig. 500 and Fig. 502 on the right demonstrate the method for a dome with no tensile capacity. Note that this method evaluates the forces directly, the stresses are obtained by dividing these values by the thickness and the width of the corresponding lune sections.

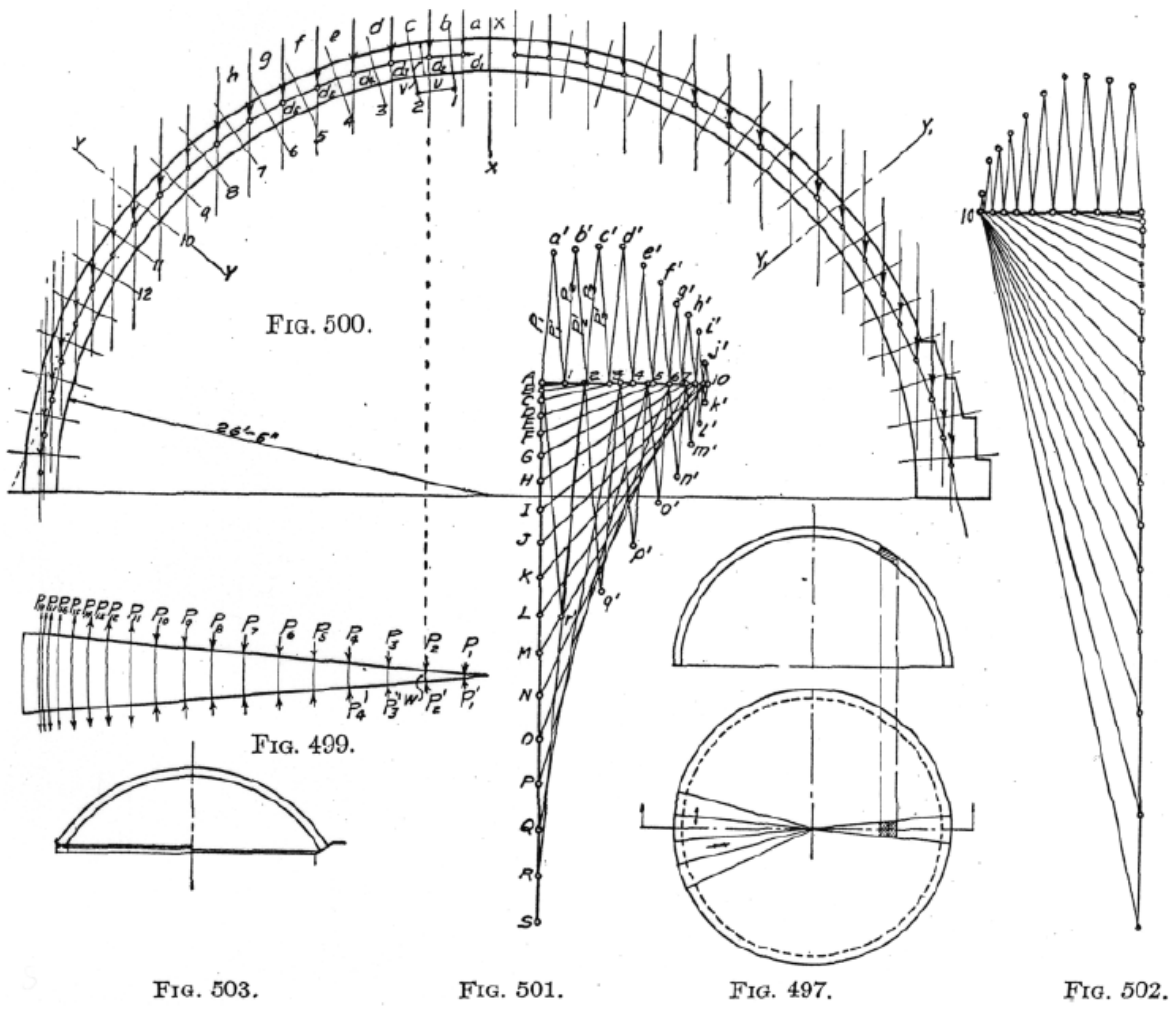

Figure 2.6: Wolfe's graphical analysis method for domes [11]

2.3.3 Finite element analysis

Finite element analysis is one of the elastic methods that can be used to analyze masonry domes. This elastic method determines the meridional and the hoop forces based on the material properties rather than its geometry. Various software programs can be used to do finite element analysis. The first step in finite element modelling is to construct a model of the structure. The model is constructed based on many user inputs, such as: Geometry of the dome, material properties (stress capacities, modulus of elasticity, poisson's ratio, etc.), boundary conditions, etc.. After running the program, the output would be the distribution and magnitude of stresses over the whole structure. Finite element modelling is very sensitive in terms of material properties and boundary conditions, thus accurate inputs are necessary to ensure reliable results.

2.3.4 Equilibrium methods vs. finite element methods

Equilibrium methods assess the stability of masonry domes based on their geometry and using equilibrium equations. These methods determine the hoop and meridional forces, the thrust reaction at the base of the dome, and a possible thrust line along the dome. Based on the safe theorem, if at least one possible thrust line is determined within the thickness of the dome, then the dome is considered to be safe and stable. Equilibrium methods have always been used in the past in the design of historic masonry domes and so proved their credibility as an analysis technique.

Elastic methods by finite element analysis determines the hoop and meridional forces based on the strength of the material. Forces within the dome are determined based on the boundary conditions and imposed deformations of the dome. Finite element solutions are elastic and are sensitive to any small movements of the supports. Such small movements are bound to occur and so the the exact stress state of the dome is difficult to evaluate. Additionally, masonry domes undergo tensile hoop forces towards the base of the dome, and so induces cracking. And cracks makes finite element methods inadequate to evaluate the stress state of domes after cracking. For these reasons, the approach used in this thesis will be based on equilibrium methods rather than elastic methods.

2.4 Guastavino Sr. and masonry tiles

In 1892, Rafael Guastavino Sr. published a book named Essay on the Theory and History of Cohesive Construction. [2] The book summarizes all of his theories about masonry tile behaviour, mechanical properties, design methodologies, and construction techniques. One of the most interesting points in the book is the idea of cohesion of the tiles. He suggested that tile vaults act as a solid mass rather than sliced arches or domes. This cohesion would give the tile vaults a much greater shear and tensile capacity than sliced arches. He conducted mechanical tests to find the values of these capacities, and the results are listed in Table 2.1.

Because of the existence of this tensile capacity in the vaulting tiles, Guastavino suggested that domes do not thrust outwards at the base. He said that this thrust would be taken by the tensile capacity of the tiles, and that would act as a natural tension tie. In his book, Guastavino suggested that, when designing a Guastavino dome, a steel ring should be included at the base of dome, though he did not mention that

the steel ring counteracts the thrust of the dome. [12] Guastavino's understanding of how masonry domes behave might not have been completely correct, but his intuition was right enough to include tension rings when designing masonry domes. This topic will be further touched upon in §4.3

Table 2.1: Masonry strength results obtained from mechanical tests performed by Guastavino Sr. [13]

Strength Type	Strength Value (*psi*)
Compressive Strength, 5-day	2060
Compressive Strength, 360-day	3290
Tensile Strength	287
Transverse (Bending) Strength	90
Shear Strength, Portland Cement	124
Shear Strength, Plaster of Paris	34

Although Guastavino's mechanical tests proved that there is adequate tensile capacity for masonry tiles, one should not be tempted to leverage that capacity in masonry dome design. Huerta [14] performed a comprehensive study of the analysis and design of masonry tile vaults. He concluded that masonry tile vaulting demonstrates the same behaviour as any other masonry vaults, and so shall be analyzed with the same fundamental assumptions. Thus, the equilibrium methods with the three basic assumption of infinite compressive strength, no tensile strength, and no failure by sliding are applicable on Guastavino domes analysis.

2.5 Summary

§2 provided an overview of the basic structural analysis principles, and the most relevant principles behind the analysis of masonry structures. The analysis of such structures can be approached by either equilibrium methods or by elastic methods. The former depends on the geometry and self-weight of the structure to determine its stability, while the latter evaluates the structure based on its material strength and elasticity. Both of these methods approach the analysis from different perspectives, and which is better is an ongoing debate. This section provided a logical conclusion that the equilibrium methods are better suited to analyze masonry domes compared to elastic methods. Thus, only the equilibrium methods will be used for the analysis throughout this thesis. The last part of §2 provided the material strength properties for the Guastavino masonry tiles. These values will be referred to later on in the cathedral analysis section.

3 Analysis of a generic dome

In this section, a generic Guastavino dome will be analyzed using the equilibrium analysis methods. The three equilibrium methods that will be used are membrane analysis, Wolfe's graphical analysis assuming tensile capacity for the dome, and Wolfe's graphical analysis assuming no tensile capacity for the dome. The purpose of these analyses on a generic dome is to calculate and compare the results between the different analysis methods, discuss the applicability of each method, and determine which method is the most appropriate to use for the analysis of the dome of the Cathedral of Saint John the Divine.

The geometry and properties of the generic dome mimic that of a typical Guastavino dome. The spherical dome has a radius, r, of 65 ft and a thickness, t, of 4 in, and the angle from the vertical down to the base of the dome is 70°. The density of the Guastavino tiles used in this analysis is 112 pcf. [15] The properties of the generic masonry dome are summarized in Table 3.1, and shown in Figure 3.1.

Table 3.1: Properties of the generic masonry dome

Property	Value
Radius, r	65 ft
Thickness, t	4 in
Angle, ϕ	70°
Density, ρ	112 pcf

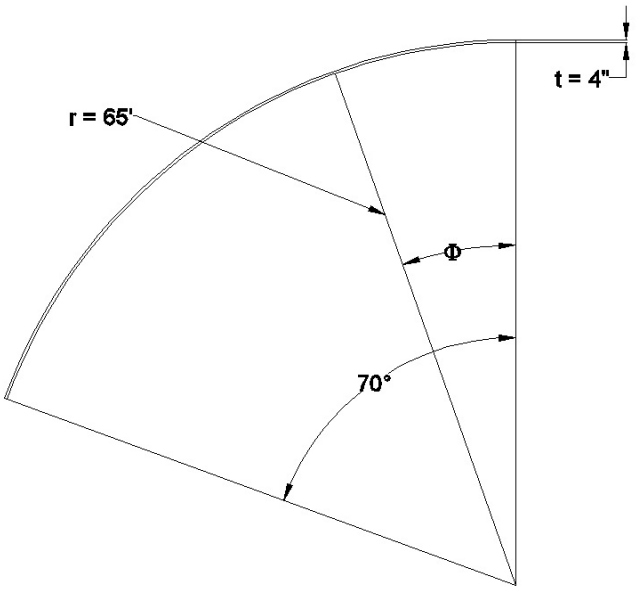

Figure 3.1: A cross-sectional view of one half of the dome

3.1 Membrane analysis

As was mentioned in §2.3.1, the purpose of the membrane analysis method is to determine the meridional and hoop forces within a lune section of a dome. In this generic dome analysis, the longitudinal width angle of the lune, θ, was chosen to be 15° along the length of the lune from the top towards the bottom. This lune section will be divided into ten latitudinal sections, each having a latitudinal angle, ϕ, of 7°. Figure 3.2 shows the cross-sectional lune that will be analyzed, and Figure 3.3 shows one of the ten sections along the cross-sectional lune. Each section will be analyzed as a surface, and using the two membrane analysis equilibrium equations, the meridional, N_ϕ, and hoop, N_θ, stresses can be calculated.

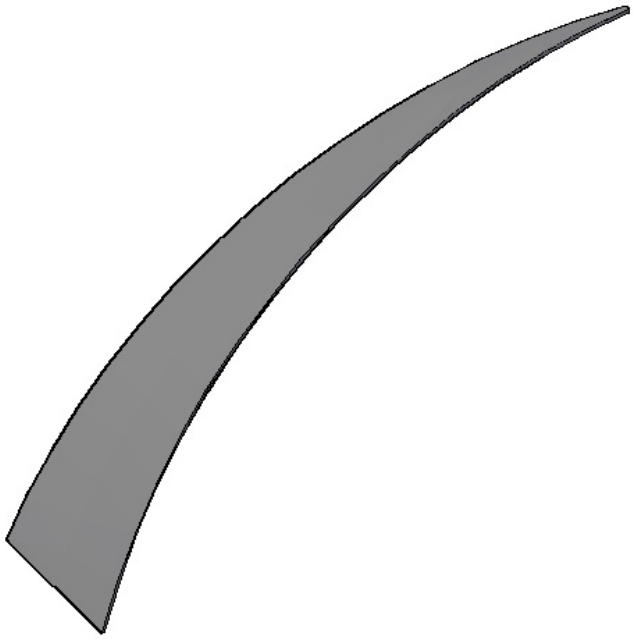

Figure 3.2: A cross-sectional lune with $\theta = 15°$

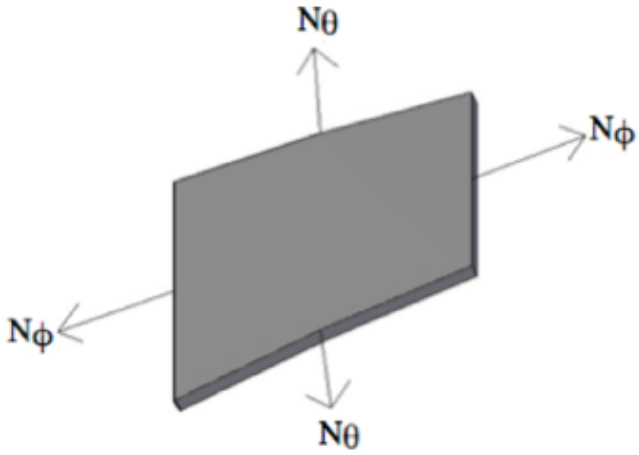

Figure 3.3: One of the ten sections along the cross-sectional lune

N_ϕ and N_θ can be calculated using the two equilibrium equations 3.2 and 3.1. Where r is the radius of the dome and is equal to 65 ft for the generic dome. w is the weight per unit area for each section of the lune, and is equal to ρt.

$$N_\phi = -\frac{wr}{1+\cos(\phi)} \tag{3.1}$$

$$N_\theta = wr\,(\frac{1}{1+\cos(\phi)} - \cos(\phi)) \tag{3.2}$$

These two equations have been applied for each of the ten sections along the length of the lune, and the results of the calculations are shown in Table 3.2 and Table 3.3.

Table 3.2: Meridional stresses and forces from membrane analysis on the generic dome

ϕ (°)	Stress (psf)	Force (lb)
0	-3640	
7	-3654	-2554
14	-3695	-5127
21	–3765	-7739
28	-3866	-10411
35	-4002	-13166
42	-4176	-16029
49	-4396	-19030
56	-4669	-22203
63	-5007	-25589
70	-5425	-28989

Table 3.3: Hoop stresses and forces from membrane analysis on the generic dome

ϕ (°)	Stress (psf)	Force (lb)
0	-3640	-9635
7	-3572	-9456
14	-3369	-8918
21	-3031	-8024
28	-2562	-6781
35	-1962	-5192
42	-1234	-3266
49	-380	-1006
56	598	1583
63	1702	4505
70	2935	

The results from the generic dome analysis are as expected. The meridional forces are minimum in compression at the crown of the dome ($\phi = 0°$), and increases in compression towards the base of the dome ($\phi = 70°$). The hoop forces are maximum in compression at the crown of the dome ($\phi = 0°$), and decreases in compression until it reaches the neutral axis ($\phi = 51.82°$), and then increases in tension towards the base of the dome ($\phi = 70°$).

3.2 Graphical analysis

As the name implies, graphical analysis methods are based on drawing a cross-sectional lune for half of the dome. From there, one can determine the hoop and the meridional forces along the lune. An identical lune to that analyzed using membrane analysis, will be analyzed using graphical analysis . The lune, which has a longitudinal width, θ, of 15°, will be divided into ten sections, and the meridional and hoop forces will be determined for each section. The graphical analysis methods that will be applied are the ones developed by Wolfe. [11]

3.2.1 Wolfe's graphical analysis assuming tensile capacity for the dome

This graphical analysis method assumes there is tensile capacity for the masonry dome. The tensile stresses are necessary to calculate if steel ties are introduced in the tensile hoop stresses zone. In a matter of fact, this is the case for the dome of the Cathedral of Saint John the Divine, as will be explained in details in §4.3. Figure 3.4 shows the cross-sectional lune, and the red line represents the meridional thrust line along the lune. This thrust line is at the mid-surface of the dome's thickness.

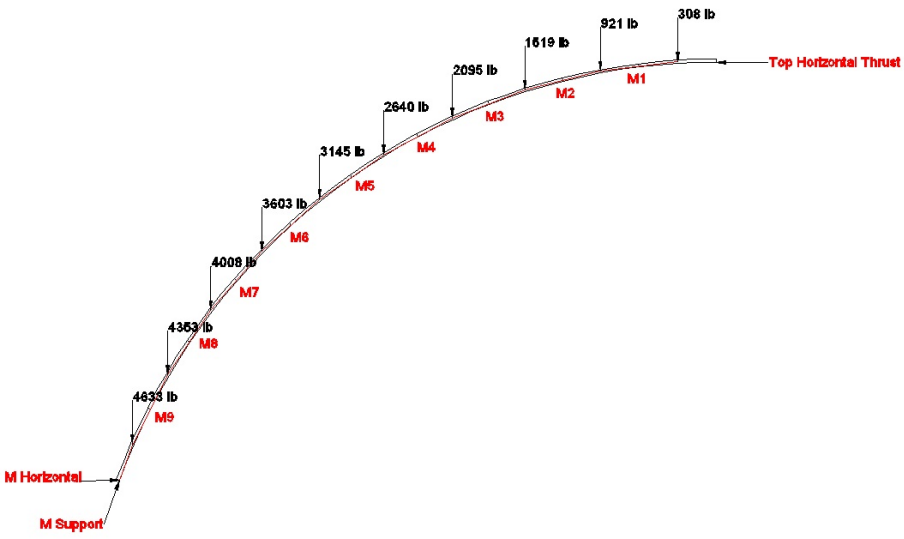

Figure 3.4: A cross-sectional lune showing the meridional thrust lines

The weight, w, of each section along the lune has been calculated using equation 3.3, where $\theta = 15°$, R_o and R_i are the outside and inside radius of the dome, and ϕ_2 and ϕ_1 are the bottom and top latitudinal angle of

the section, respectively. The properties and weights of each section are presented in Appendix B.

$$w = \rho g \int \int \int_v r^2 \sin(\phi)\, dr\, d\theta\, d\phi \tag{3.3}$$

This integral yields an answer of:

$$w = \rho g \frac{\theta}{3}(R_o^3 - R_i^3)(\cos(\phi_1) - \cos(\phi_2)) \tag{3.4}$$

Figure 3.5 shows the force polygon produced using Wolfe's graphical analysis method with tensile capacity. The red lines represent the meridional forces, and the green lines represent the hoop forces. The size of each line is proportionally scaled to the size of the corresponding hoop or meridional force. Figure 3.6 shows a plan view of the lune, with the corresponding locations of the hoop forces. The hoop forces are assumed to be applied at the mid-point of each section along the lune. The results of the forces for each of the ten sections are summarized in Table 3.4 and 3.5. Both of the results are as expected, and the trend of the hoop and the meridional forces is similar to that of the membrane analysis.

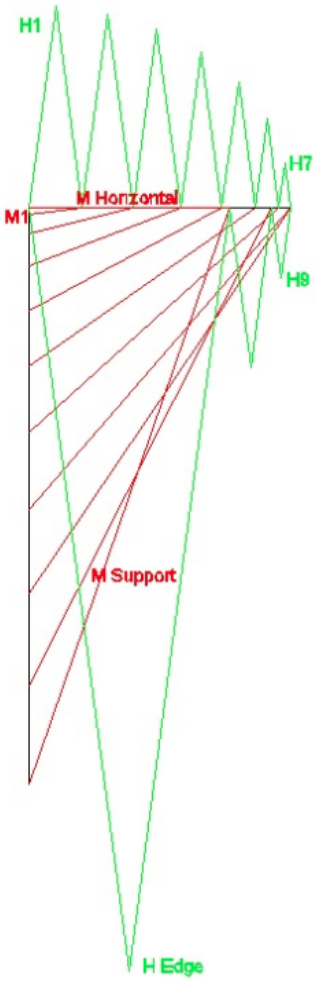

Figure 3.5: Force polygon of the generic dome using Wolfe's graphical analysis assuming tensile capacity for the dome

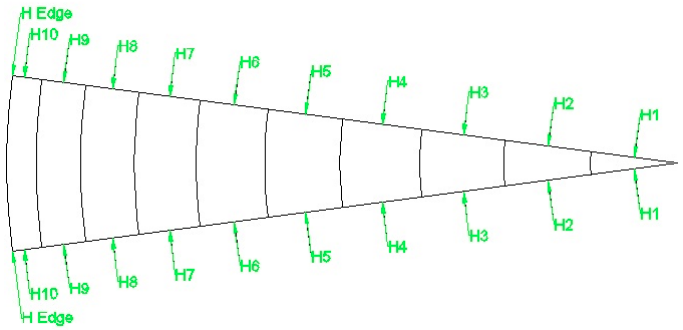

Figure 3.6: Plan view of the lune showing the locations of the hoop forces using Wolfe's graphical analysis assuming tensile capacity for the dome

Table 3.4: Meridional stresses and forces of the generic dome using Wolfe's graphical analysis assuming tensile capacity for the dome

Section	ϕ (°)	Stress (psf)	Force (lb)
Top Horizontal Thrust	0		-2510
M1	7	-3618	-2529
M2	14	-3658	-5077
M3	21	-3728	-7663
M4	28	-3828	-10309
M5	35	-3962	-13036
M6	42	-4135	-15871
M7	49	-4353	-18843
M8	56	-4632	-22027
M9	63	-4958	-25337
M Support	70	-5395	-28833
M Horizontal			-9495

Table 3.5: Hoop stresses and forces of the generic dome using Wolfe's graphical analysis assuming tensile capacity for the dome

Section	ϕ (°)	Stress (psf)	Force (lb)
H1	3.5	-3632	-9615
H2	10.5	-3496	-9254
H3	17.5	-3224	-8533
H4	24.5	-2817	-7458
H5	31.5	-2279	-6033
H6	38.5	-1610	-4263
H7	45.5	-814	-2154
H8	52.5	0	0
H9	59.5	1272	3368
H10	66.5	2859	7568
H Edge	70		36373

3.2.2 Wolfe's graphical analysis assuming no tensile capacity for the dome

This method is identical to that in §3.2.1, except that it takes a zero value for all the tensile hoop forces. With that, the meridional forces values in the tensile hoop stresses region are slightly larger, and the meridional forces thrust lines in the tensile hoop region are more deviated outwards. Figure 3.7 shows the force polygon produced using this analysis method. Figures for the meridional thrust lines and a plan view of the segmented lune are not shown here because they are almost identical to those in §3.2.1.

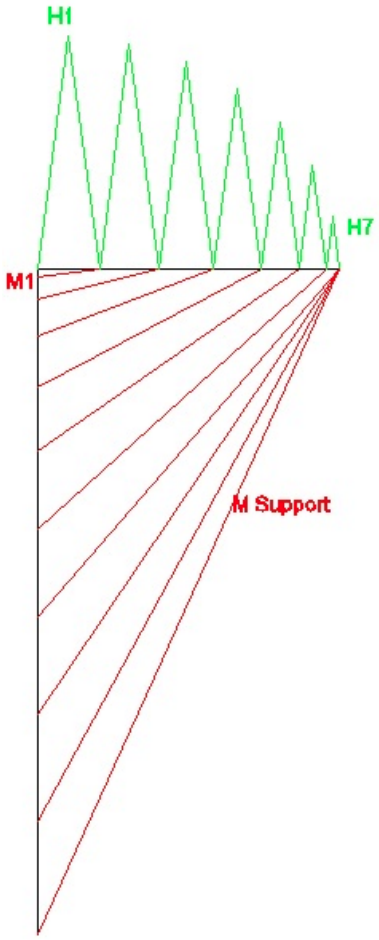

Figure 3.7: Force polygon of the generic Guastavino dome using Wolfe's graphical analysis assuming no tensile capacity for the dome

The results of the forces for each of the ten sections are summarized in Table 3.6 and 3.7. Both of the results are as expected, and the trend of the hoop and the meridional forces is similar to that of the membrane analysis and the other Wolfe's graphical analysis method. Please note that the there are no tensile hoop forces, and the meridional forces in the tensile hoop region are slightly larger compared to those of the other Wolfe's graphical method.

Table 3.6: Meridional stresses and forces of the generic dome using Wolfe's graphical analysis assuming no tensile capacity for the dome

Section	ϕ (°)	Stress (psf)	Force (lb)
Top Horizontal Thrust	0		-2510
M1	7	-3618	-2529
M2	14	-3658	-5077
M3	21	-3728	-7663
M4	28	-3828	-10309
M5	35	-3962	-13036
M6	42	-4135	-15871
M7	49	-4353	-18843
M8	56	-4632	-22027
M9	63	-5038	-25747
M Support	70	-5594	-29895
M Horizontal			-12350

Table 3.7: Hoop stresses and forces of the generic dome using Wolfe's graphical analysis assuming no tensile capacity for the dome

Section	ϕ (°)	Stress (psf)	Force (lb)
H1	3.5	-3632	-9615
H2	10.5	-3496	-9254
H3	17.5	-3224	-8533
H4	24.5	-2817	-7458
H5	31.5	-2279	-6033
H6	38.5	-1610	-4263
H7	45.5	-814	-2154
H8	52.5	0	0
H9	59.5	0	0
H10	66.5	0	0
H Edge	70		0

3.3 Discussion of the analysis results

The results of the forces and stresses from all three analysis methods gave expected and similar results. Figure 3.8 shows the meridional forces from all three analysis methods. The figure shows the trend of the forces from the crown ($\phi = 0°$) till the bottom ($\phi = 70°$) of the dome. Similarly, Figure 3.9 shows the results for the hoop forces.

The results from the these graphs clearly show that all three analysis methods are consistent with each other. The general trend of the results are as expected. The meridional forces increase in compression from the crown towards the base of the dome.The hoop forces decrease in compression until the neutral axis ($\phi = 51.82°$) is reached, and then increase in tension towards the base of the dome.There is a slight difference

in the results towards the base of the dome. This may be the result of the larger mass of the lune sections towards the base, thus a larger chance of error and variation between the different methods. Nonetheless, the results are consistent

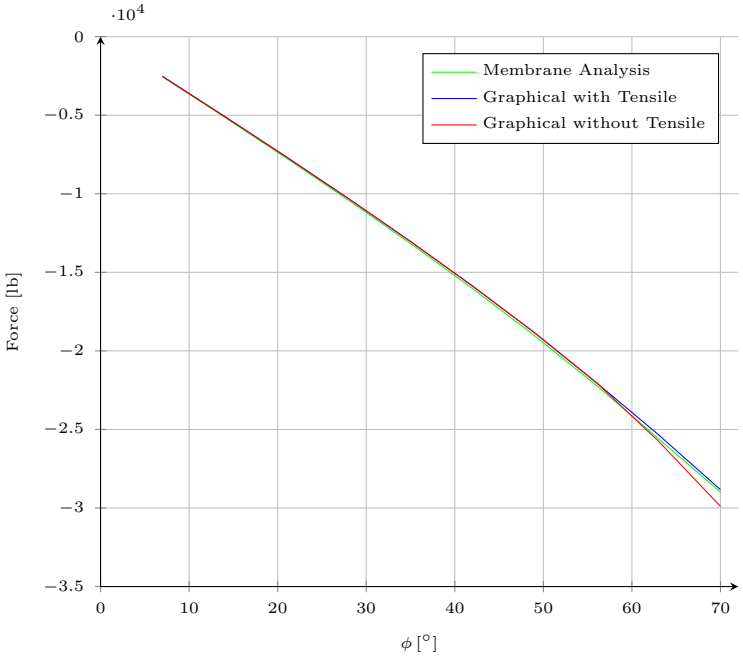

Figure 3.8: Results comparison of the meridional forces of the generic dome

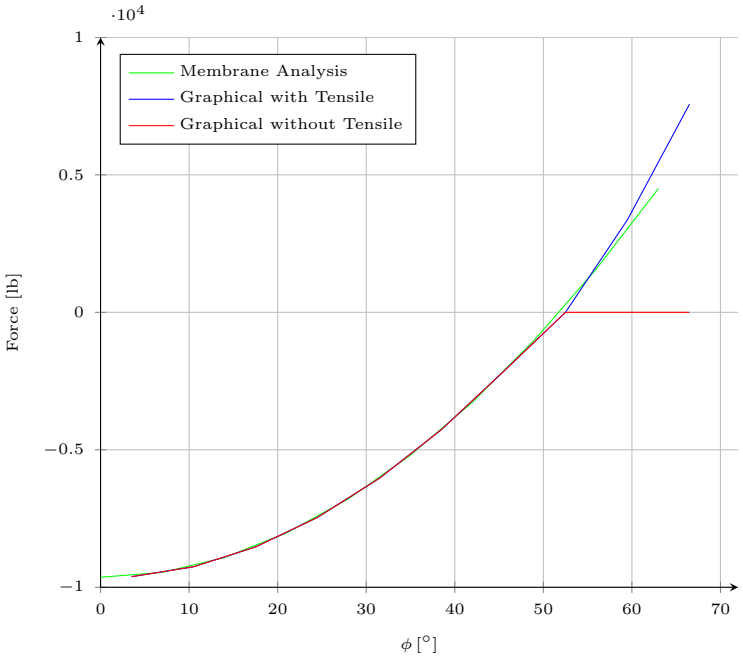

Figure 3.9: Results comparison of the hoop forces of the generic dome

The results obtained from this analysis can be compared to the masonry strength results obtained from the mechanical tests performed by Guastavino Sr., as shown in Table 2.1. The maximum compressive stress from all the analysis results is 5,594 *psf* (Table 3.6) and this is equivalent 39 *psi*. The maximum tensile stress is 2,935 *psf* (Table 3.3) and this is equivalent to 20 *psi*. These values are much lower than the 5-day compressive strength (2,060 *psi*) and tensile strength (287 *psi*) determined by Guastavino Sr., as shown in Table 2.1. This implies that Guastavino domes can easily take up the dead loads of its self-weight. These results imply that the dome itself is sufficient to resist all the tensile stresses acting on it. Regardless, steel ties may be installed at the base of the dome to take on the hoop tensile stresses. This is the case for the dome of the cathedral, as will be discussed in details in §4.3.

3.4 Summary

The results from all three analysis methods are consistent with each other. This implies that all of these equilibrium methods are effective in analyzing and evaluating the meridional and hoop forces in a masonry dome. They can also be used to determine a possible thrust line from the crown to the base of a masonry dome.

In §4, a complete analysis of the forces within the masonry dome of the Cathedral of Saint John the Divine will be performed. The equilibrium methods that will be used are only the membrane analysis, and Wolfe's graphical analysis assuming tensile capacity for the dome. The masonry dome that will be studied has steel ties at the base and one of the objectives of this thesis is to evaluate the necessity of these steel ties. Wolfe's graphical analysis method assuming no tensile capacity for the dome does not calculate a value for the tensile hoop stresses, and so progressing with this method is not necessary. However, this does not imply the invalidity of its results.

4 Analysis of the dome of the cathedral

4.1 Overview of the dome

Figure 4.1: The dome [3]

An overview of the masonry dome and the pendentives is shown in Figure 4.1. All of the dome geometry and detailing have been obtained from the original Guastavino drawings, these drawings have been obtained from Avery Library. [16] The main original drawing of the dome is shown in Figure 4.2, and other detailed drawings are presented in Appendix E. The dome is spherical and has a radius of 66 *ft*, and a diameter of 98 *ft* at the base, where it rests on the pendentives, which are spherical triangles of the same radius. The bottom of the pendentives is 95 *ft* above the ground and the total rise to the top of the dome is 66 *ft*, making the the crown of the dome 161 *ft* above the ground. The dome is incredibly thin with a L/t ratio of around 200. This dome is relatively twice as thin compared to an egg which has a L/t ratio of 100.

The thickness of the dome gradually increases from the crown towards the base of the dome. The thinnest part of the dome was constructed using 3 courses, giving a total thickness of 4 *in*. The thickness segmentally increases to 4 and 5 courses, corresponding to thicknesses of 6, and 7.5 *in*, respectively. The pendentives are then extended towards the base at the four corners of the dome. The pendentives have a uniform thickness of 9 courses, or about 12 in. The four great arches have a uniform cross section of 12x12 ft^2 and form a square perimeter around the dome. These arches are responsible for taking the thrust from the dome and the pendentives towards the four main piers.

It was determined that the most effective way to analyze the flow of forces of the dome is to study two cross sections within the dome, as shown in Figure 4.3. The first section, named *cross section*, goes from the crown to the base of the dome, having an embrace angle (ϕ) of 45°. And the other section, named *diagonal section*, goes from the crown of the dome towards the bottom of the pendentives, having a total embrace angle (ϕ) of 78° . It was necessary to perform two separate analysis because the diagonal section is thicker towards its base compared to that of the cross section, thus the magnitude of forces will be different. Full details and dimensions of the cross section and the diagonal section are shown in the cross-sectional view of half the dome in Figure 4.4.

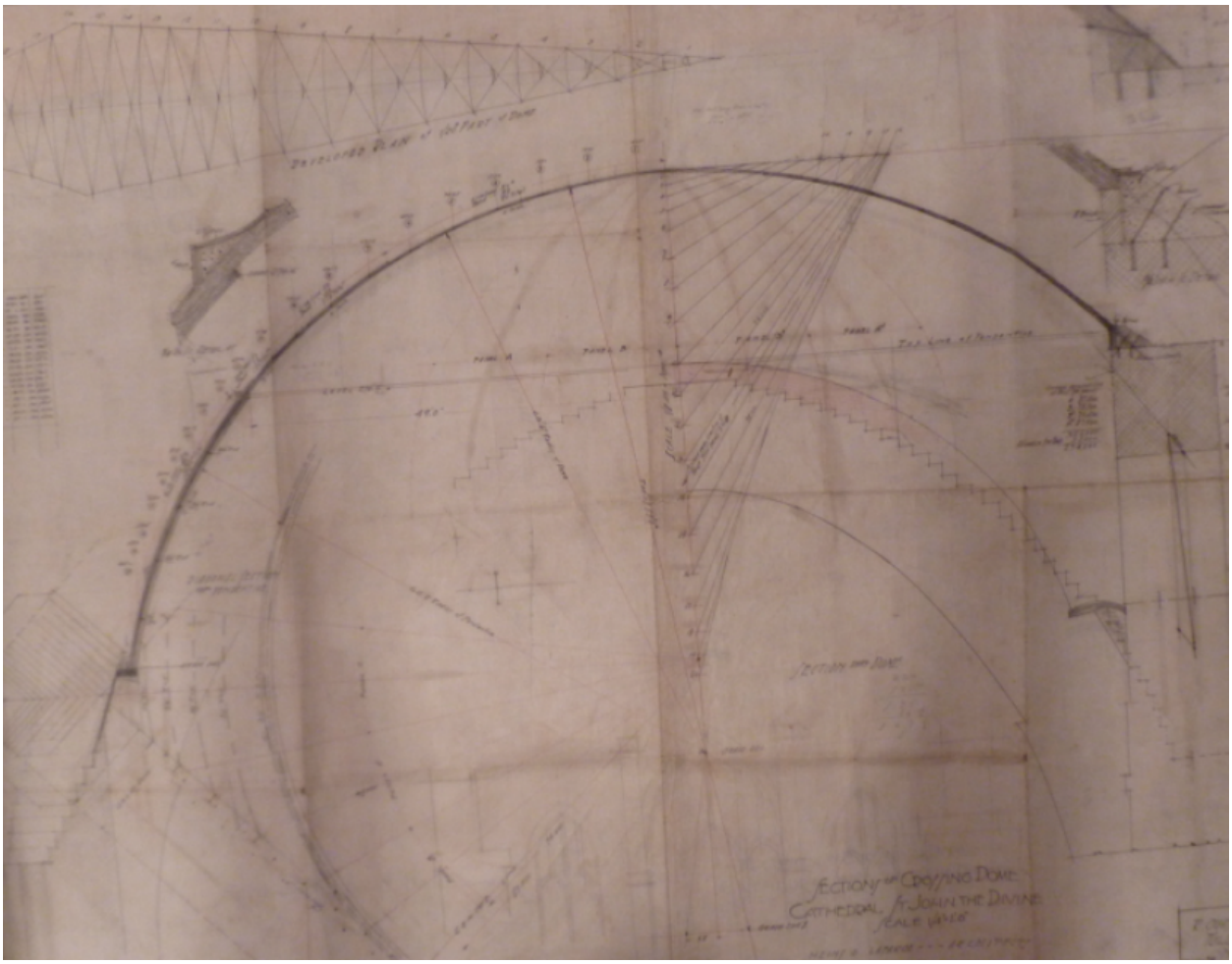

Figure 4.2: Original Guastavino drawing of the dome [16]

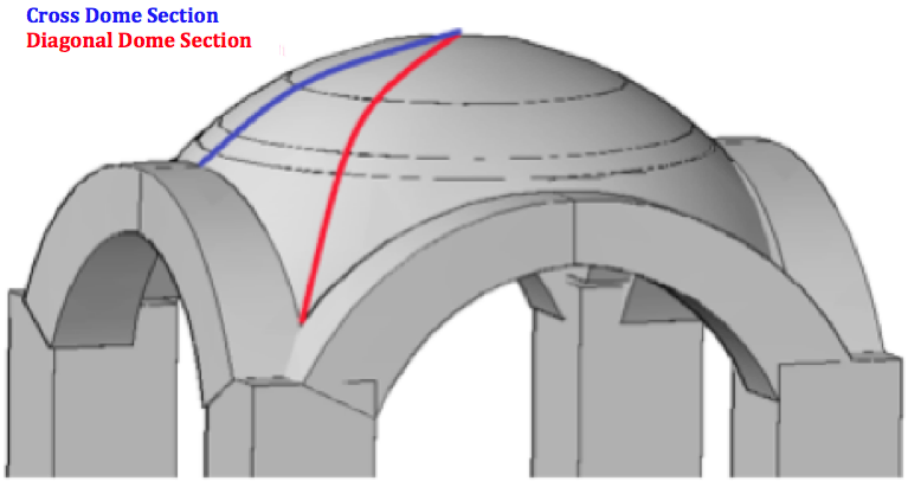

Figure 4.3: Dome Analysis Sections

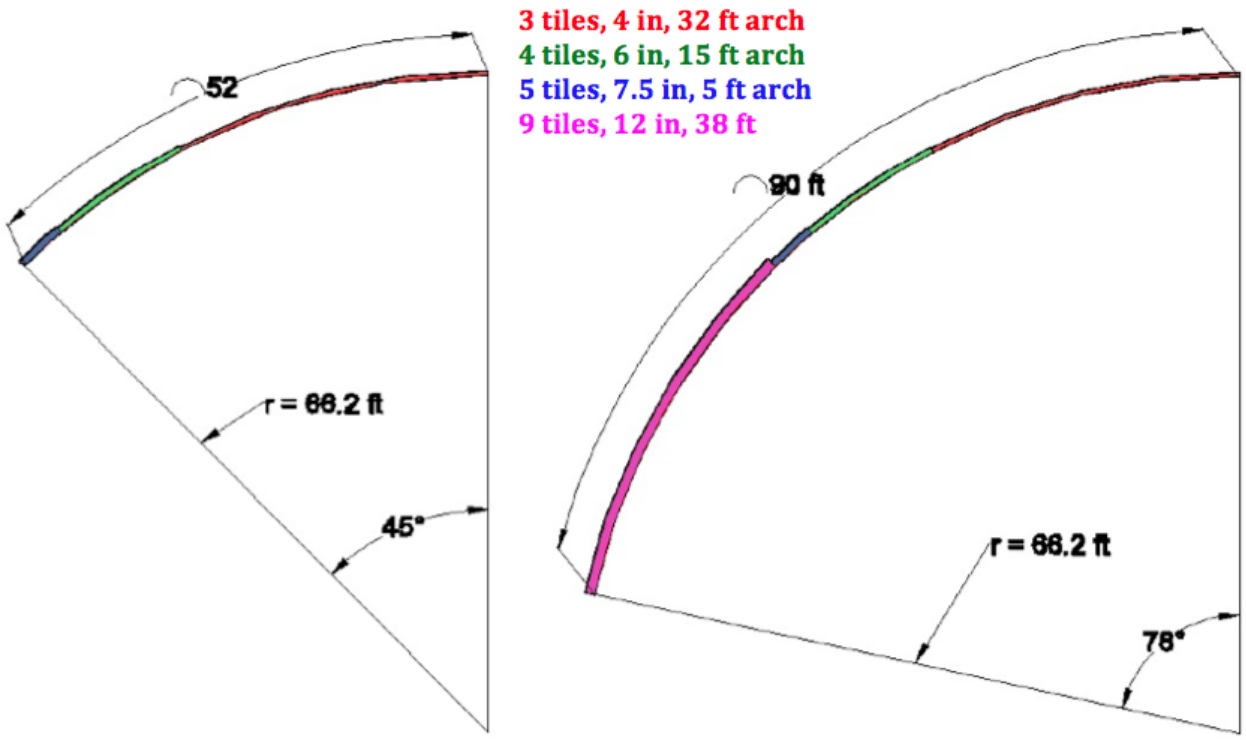

Figure 4.4: A cross-sectional view of the cross dome (left) and diagonal dome (right)

4.2 Symmetric loading

The self-weight is symmetrical across the whole dome. This implies that analyzing a cross-section of half the dome should be sufficient to get a sense of the forces through the whole dome. The assessment will be done using membrane analysis and graphical analysis, and then the results will be compared and discussed.

4.2.1 Membrane analysis

The methodology of the membrane analysis has been explained and applied on the generic dome in §3.1 This method assumes that the dome is an infinitely thin shell at the mid-thickness of the dome. A lune section will be taken across the dome, similar to that shown in Figure 3.2. The longitudinal width angle (θ) of this lune was taken to be 15°. This lune will be divided into 12 sections for the cross dome (each with a latitudinal angle, $\phi = 3.8°$). The lune of the diagonal dome is taken with the same longitudinal width as that of the cross dome. This lune is divided into 21 sections, each has the same latitudinal angle as that of the cross dome section. With these specifications, one can determine the meridional and hoop stresses using these equations:

$$N_\phi = -\frac{wr}{1+\cos(\phi)} \tag{4.1}$$

$$N_\theta = wr\ (\frac{1}{1+\cos(\phi)} - \cos(\phi)) \tag{4.2}$$

Tables 4.1 and 4.2 summarize the results of these calculations for both the cross and the diagonal section of the dome.

Table 4.1: Cross dome lune: Meridional and hoop forces and stresses using membrane analysis

	Meridional		Hoop	
ϕ (°)	Stress (psf)	Force (lb)	Stress (psf)	Force (lb)
0.0	-3715		-3715	-5322
3.8	-3719	-1409	-3695	-5294
7.5	-3731	-2820	-3636	-5209
11.3	-3750	-4250	-3538	-5069
15.0	-3778	-5664	-3402	-4873
18.8	-3815	-7089	-3226	-4621
22.5	-3860	-8540	-3012	-4314
26.3	-3914	-10028	-2759	-4944
30.0	-3980	-14420	-2471	-5315
33.8	-4057	-19607	-2145	-4613
37.5	-4142	-21975	-1779	-3981
41.3	-4239	-25352	-1378	-3705
45.0	-4352	-33590	-940	

Table 4.2: Diagonal dome lune: Meridional and hoop forces and stresses using membrane analysis

	Meridional		Hoop	
ϕ (°)	Stress (psf)	Force (lb)	Stress (psf)	Force (lb)
0.0	-3715		-3715	-5293
3.8	-3719	-1453	-3695	-5265
7.5	-3731	-2655	-3636	-5181
11.3	-3750	-4070	-3538	-5041
15.0	-3778	-5495	-3402	-4846
18.8	-3815	-6932	-3226	-4596
22.5	-3860	-8386	-3012	-4291
26.3	-3914	-9858	-2759	-3932
30.0	-3980	-14209	-2471	-4403
33.8	-4057	-19356	-2145	-4588
37.5	-4142	-21689	-1779	-3807
41.3	-4239	-25041	-1378	-3066
45.0	-4352	-33181	-940	-2514
48.8	-4483	-49484	-466	-1695
52.5	-4628	-63476	46	196
56.2	-4783	-68839	594	2544
59.9	-4958	-74394	1180	5047
63.6	-5153	-80160	1801	7707
67.3	-5372	-86164	2461	10528
71.0	-5617	-92435	3159	13514
74.2	-5892	-69185	3897	16673
78.0	-6164	-49346	4586	

The general trend of the results is as expected, however there is some fluctuations in some values. These fluctuations must be due to the change in the thickness along the dome, as will be further discussed in §4.2.3. Regardless, the meridional forces gradually increases in compression, and the hoop forces decreases in compression till the neutral axis is reached ($\phi = 51.82°$) and then increases in tension. What is interesting about the cross dome section is that the maximum ϕ at the bottom is 45°; this means that hoop forces will always be in compression, and this is confirmed as shown in Table 4.1. The theoretical implication of this is that no tension steel ties are necessary at any point in the spherical dome above the supporting arches level, even at its base. This is not the case in reality as will be discussed further in §4.3.

4.2.2 Graphical analysis

The graphical analysis method that will be used for the dome of the cathedral is Wolfe's graphical analysis assuming tensile capacity for the dome. It is necessary to use this method in order to calculate what are the tensile hoop forces so as to evaluate the necessity of the steel ties in the dome. Based on the same reason, it would not be effective to use the other Wolfe's graphical method as it does not calculate a value for the tensile hoop forces. The methodology of this method is exactly as described in §3.2.1. This analysis method will be applied on both the cross dome lune and on the diagonal dome lune. The dimensions of the lunes

used for this analysis are identical to those used for the membrane analysis. The properties and weights of each section for both lunes are presented in Appendix F.

Figures 4.5 and 4.6 show the cross-sectional lune of the cross and diagonal dome. These figures display the meridional thrust lines and the weights of each section within the lune. The meridional thrust lines are at the mid-surface within the dome's thickness.

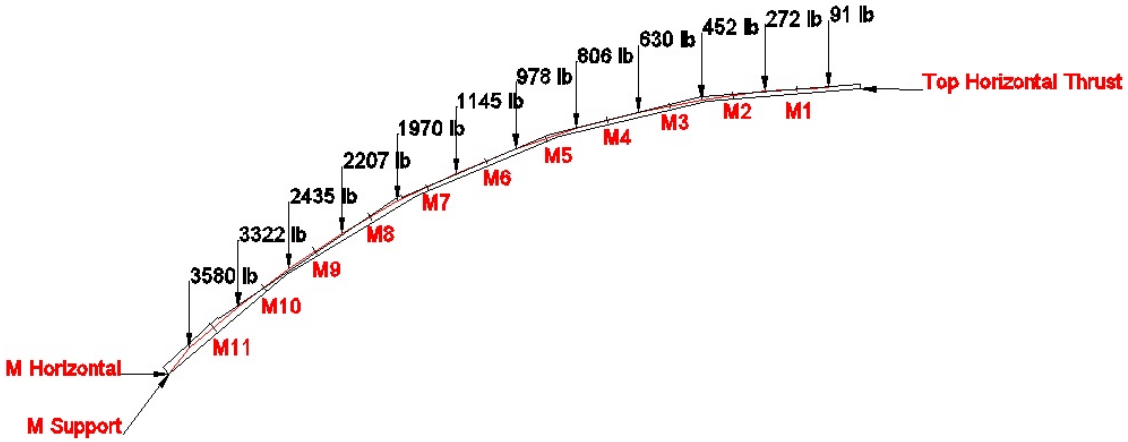

Figure 4.5: A cross-sectional view of the cross lune showing the meridional thrust lines

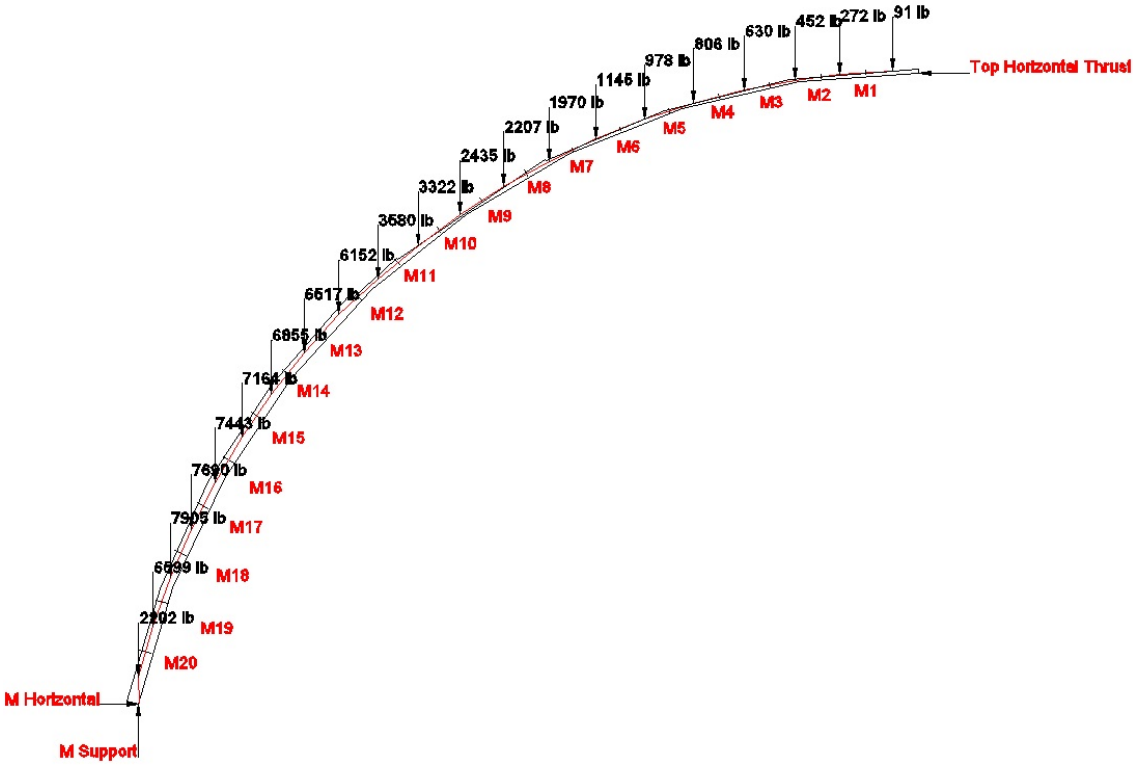

Figure 4.6: A cross-sectional view of the diagonal lune showing the meridional thrust lines

Figure 4.7 shows the force polygon of the cross and the diagonal cross-sectional lunes. The red lines represent the meridional forces and the green lines represent the hoop forces. The size of each line is proportionally scaled to the size of the corresponding hoop or meridional force.

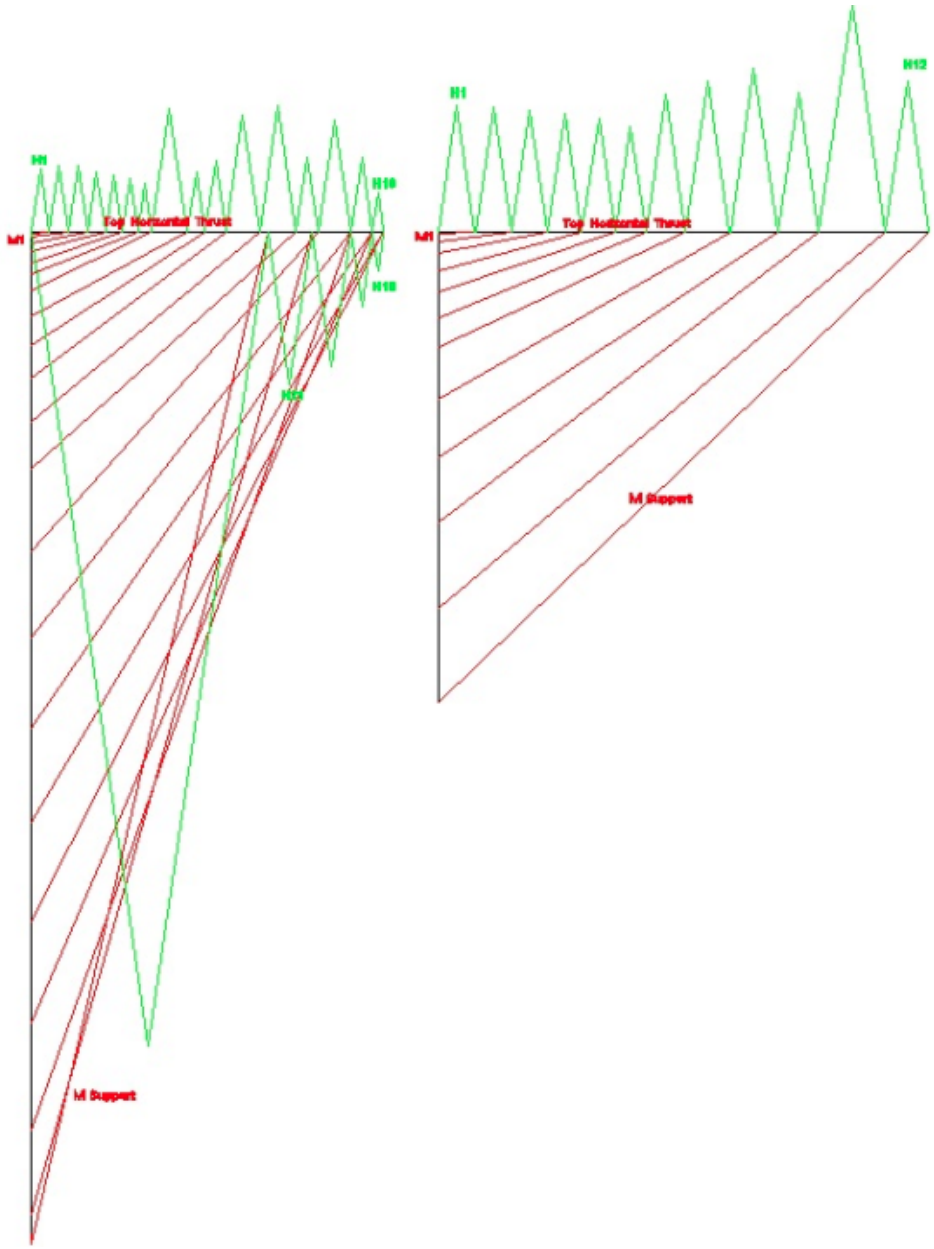

Figure 4.7: Force polygon of the diagonal (left) and cross (right) lunes

Figures 4.8 and 4.9 show a plan view of the cross and diagonal lune, with the corresponding locations of the hoop forces. The hoop forces are assumed to be applied at the mid-point of each section along the lune. Please note the last two sections for the diagonal lune are decreasing in width. This is because, at that location, the lune is being confined at the corner between the two supporting arches.

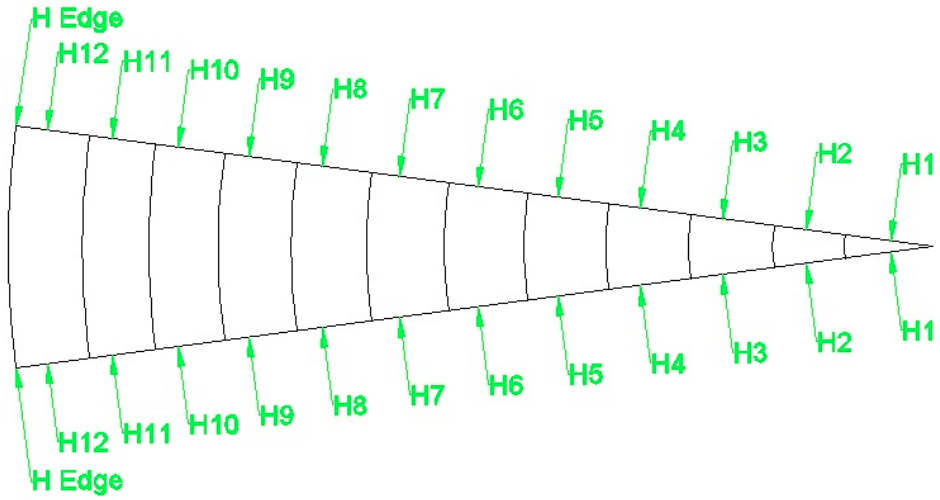

Figure 4.8: Plan view of the cross lune showing the locations of the hoop forces using graphical analysis method

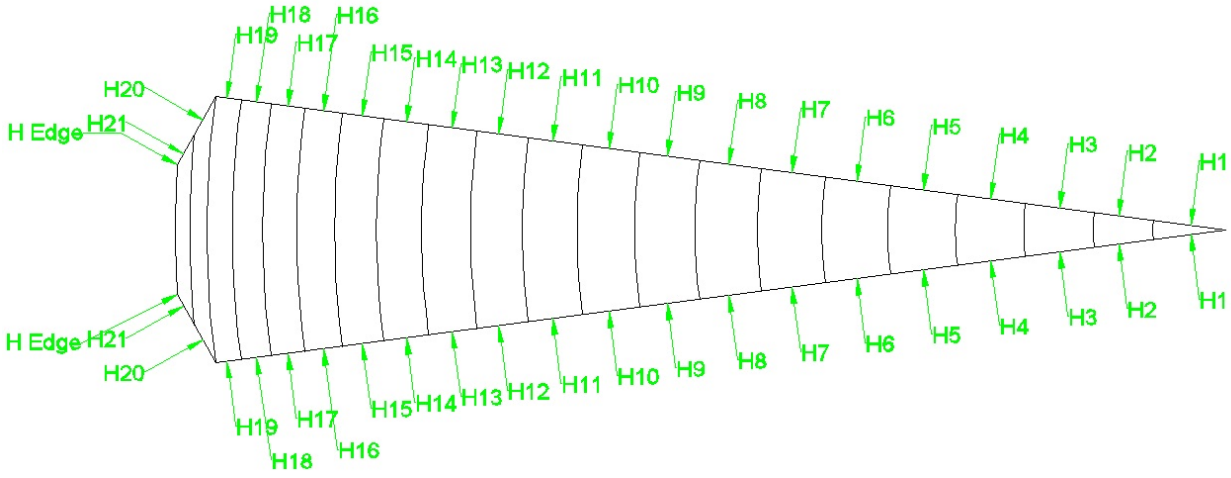

Figure 4.9: Plan view of the diagonal lune showing the locations of the hoop forces using graphical analysis method

The general trend of hoop and meridional forces are as expected. However, there are often some fluctuations in the trend of the hoop forces. This must be due to the change in the thickness along the length of the dome. These fluctuations are most obvious for the force polygon of the diagonal cross section, as shown in Figure 4.7. Table 4.3 summarizes the results of the graphical analysis calculations for both the cross and diagonal lunes of the dome.

Table 4.3: Cross and diagonal lunes: Meridional and hoop forces and stresses using graphical analysis

Cross Lune: Meridional				Cross Lune: Hoop			
Section	ϕ (°)	Stress (psf)	Force (lb)	Section	ϕ (°)	Stress (psf)	Force (lb)
Top H. Thrust	0.0		-1393				
M1	3.8	-3686	-1396	H1	1.9	-3386	-4851
M2	7.5	-3716	-2809	H2	5.6	-3314	-4748
M3	11.3	-3719	-4214	H3	9.4	-3256	-4664
M4	15.0	-3740	-5606	H4	13.1	-3139	-4496
M5	18.8	-3788	-7039	H5	16.9	-3000	-4298
M6	22.5	-3823	-8459	H6	20.6	-2814	-4032
M7	26.3	-4025	-10311	H7	24.4	-3654	-5235
M8	30.0	-3507	-12705	H8	28.1	-3214	-5760
M9	33.8	-3180	-15369	H9	31.9	-2906	-6250
M10	37.5	-3401	-18044	H10	35.6	-2460	-5291
M11	41.3	-3685	-22039	H11	39.4	-3867	-8651
M Support	45.0	-3325	-25663	H12	43.1	-2126	-5717
M Horizontal			-18488	H Edge			-64384
Diagonal Lune: Meridional				Diagonal Lune: Hoop			
Top H. Thrust	0.0		-1380				
M1	3.8	-3541	-1383	H1	1.9	-3417	-4869
M2	7.5	-4030	-2867	H2	5.6	-3537	-5039
M3	11.3	-4027	-4371	H3	9.3	-3543	-5048
M4	15.0	-3982	-5791	H4	13.0	-3210	-4574
M5	18.8	-3972	-7217	H5	16.8	-2865	-4082
M6	22.5	-3983	-8654	H6	20.5	-3052	-4348
M7	26.3	-4013	-10109	H7	24.2	-2649	-3775
M8	30.0	-3753	-13398	H8	27.9	-5252	-9359
M9	33.8	-3283	-15662	H9	31.7	-2149	-4598
M10	37.5	-3502	-18336	H10	35.4	-2534	-5422
M11	41.3	-3792	-22398	H11	39.1	-3991	-8880
M12	45.0	-3522	-26850	H12	42.8	-3633	-9715
M13	48.8	-2932	-32358	H13	46.6	-1564	-5690
M14	52.5	-2838	-38934	H14	50.3	-2007	-8586
M15	56.2	-3157	-45434	H15	54.0	-1343	-5744
M16	59.9	-3460	-51920	H16	57.7	-682	-2917
M17	63.6	-3757	-58436	H17	61.5	0	0
M18	67.3	-4055	-65041	H18	65.2	681	2916
M19	71.0	-4363	-71795	H19	68.9	1342	5742
M20	74.2	-6573	-77181	H20	72.6	2392	10235
M Support	78.0	-9546	-76414	H21	76.4	2715	11615
M Horizontal			-15889	H Edge			62079

4.2.3 Discussion of the analysis results

Figures 4.10 and 4.11 show the meridional and hoop forces of the cross lune using both analysis methods. Similarly, Figures 4.12 and 4.13 show the same results for the diagonal lune.

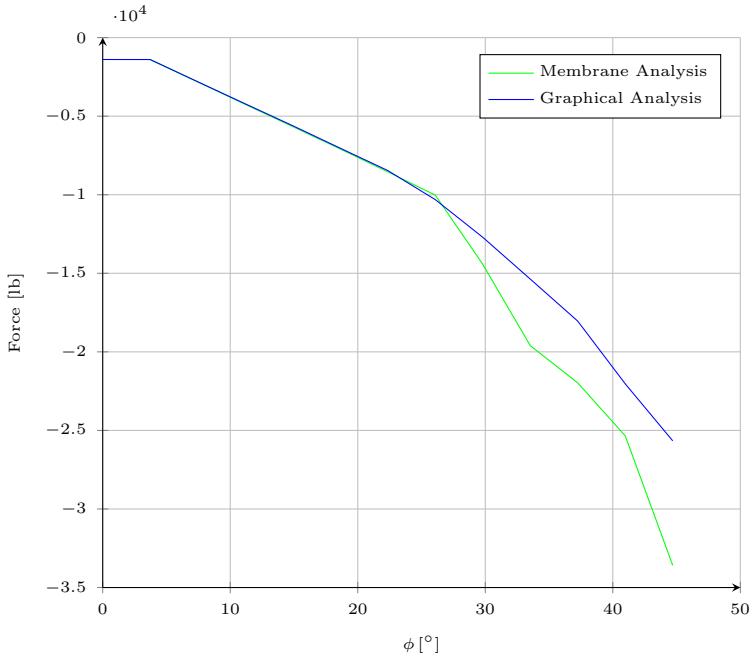

Figure 4.10: Results comparison of the meridional forces of the cross lune

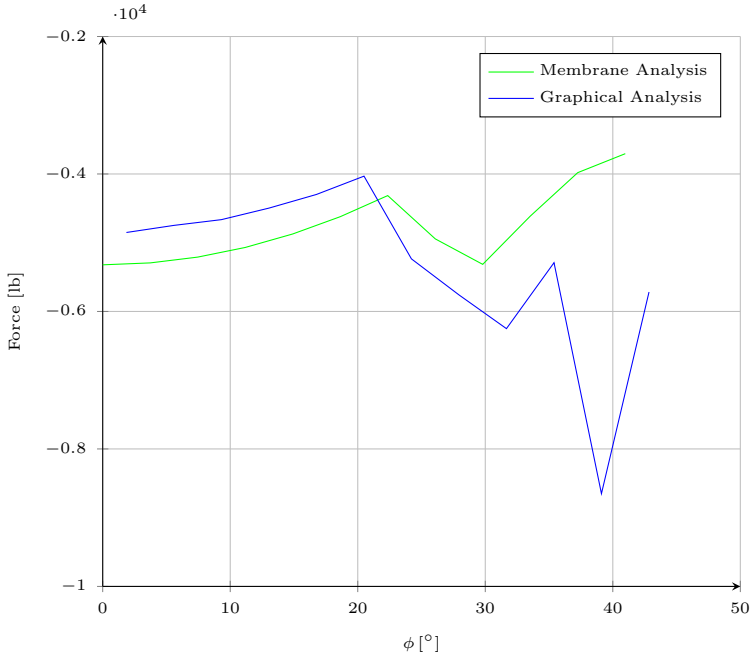

Figure 4.11: Results comparison of the hoop forces of the cross lune

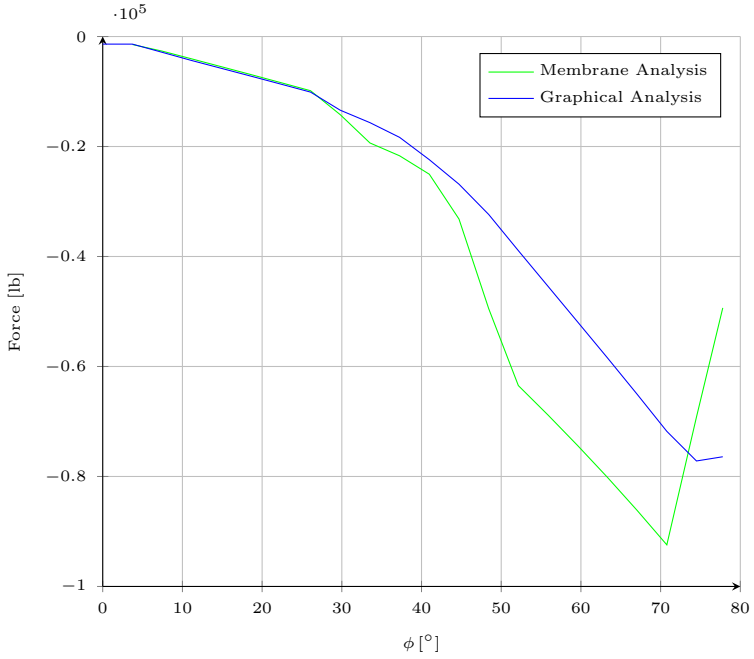

Figure 4.12: Results comparison of the meridional forces of the diagonal lune

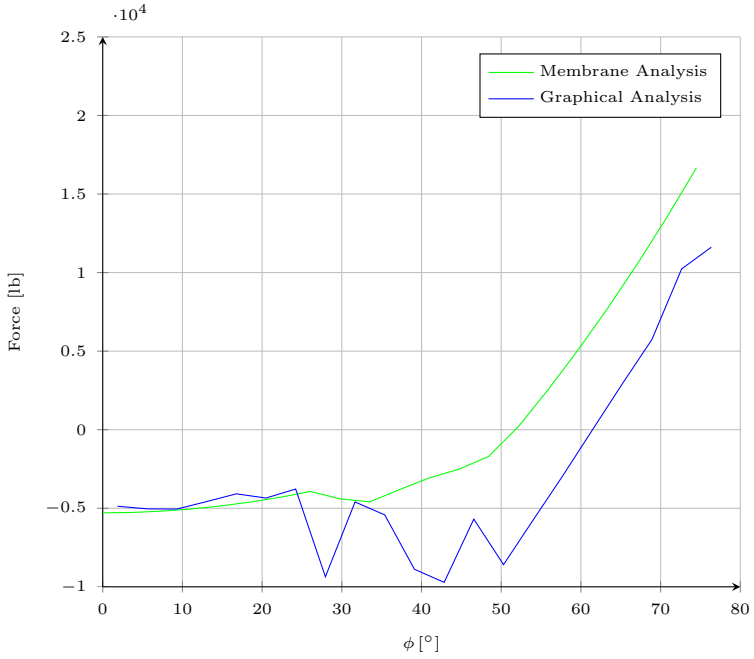

Figure 4.13: Results comparison of the hoop forces of the diagonal lune

The results of the forces and stresses from both analysis methods gave expected results with some fluctuations at some points. These fluctuations are mostly observed for the graphical analysis trends rather than that of the membrane analysis. They must be due to the fact that the thickness of the dome is segmentally changing. These fluctuations are mostly observed in Figure 4.13. The results imply that graphical analysis is more sensitive than membrane analysis to variations in the thickness of the dome. Another unexpected

fluctuation is the meridional forces of the diagonal lune obtained using the membrane analysis method, as shown in Figure 4.12. Using membrane analysis, the meridional forces are always expected to increase down the dome, but this is not the case for the diagonal lune. The reason behind that is that the width of the diagonal lune decreases towards the end of the lune section, as it is confined at the corner between the supporting arches. The forces are smaller because of the smaller width of the arch towards the end of the diagonal lune, but the stresses are still larger, as shown in Table 4.3. Another interesting observation is that the hoop forces of the diagonal lune become tensile at angle of $\phi = 60°$ rather than the theoretical angle of 52.82°, as shown in Figure 4.13. This, again, must be due to the changes in the thickness of the dome.

The results from the membrane and graphical analysis methods can be evaluated and compared, as shown in Figure 4.14. The percentage difference (%) in each of the four trends represents the difference in a specific result between both analysis methods divided by the average result. It can be observed that the percentage difference is more or less the same when there is no change in the thickness ($\phi < 23°$), and beyond that, the percentage difference increases. It can also be observed that the hoop forces are more sensitive to the change in thickness than the meridional forces. This makes sense because the hoop forces are obtained by multiplying the hoop stresses by the width and thickness of the lune sections, and so more significant fluctuations in the results would occur.

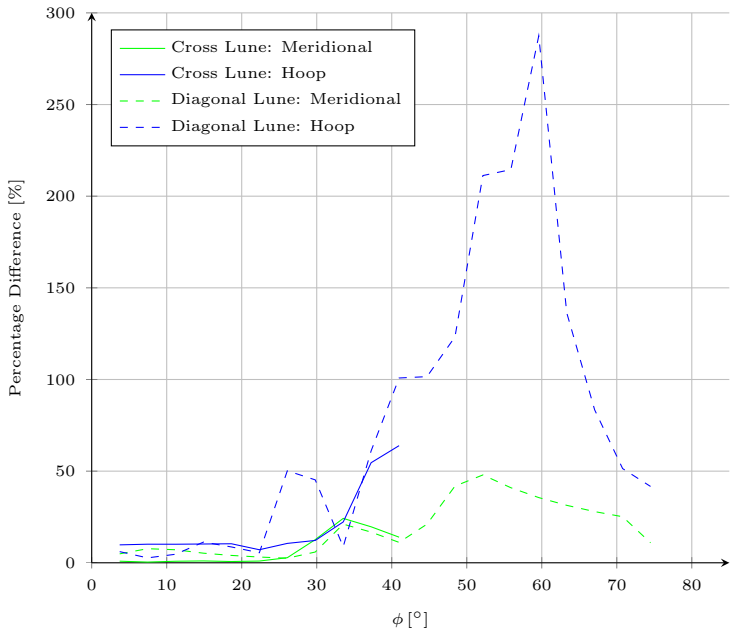

Figure 4.14: Percentage difference (%) between the results of the membrane and the graphical analysis methods

Regardless of the fluctuations, the overall trend of the results is as expected. The analysis in this section gave one possible shape of the infinitely many thrust lines within the dome. With this thrust line shape, the resulting hoop and tensile forces have been determined. These results can be compared to the masonry strength results obtained from the mechanical tests performed by Guastavino Sr., as shown in Table 2.1, to ensure the capacity of the dome. The maximum compressive stress from all the analysis results is 9,546 *psf* (Table 4.3) and this is equivalent 66 *psi*. The maximum tensile stress is 2,715 *psf* (Table 4.3) and this

is equivalent to 19 *psi*. These values are much lower than the 5-day compressive strength (2,060 *psi*) and tensile strength (287 *psi*) determined by Guastavino Sr., as shown in Table 2.1. This implies that the dome can easily take up its self-weight. These results imply that the dome itself is sufficient to resist all the tensile stresses acting on it. However, Guastavino Company always introduced steel ties at the base of the dome to resist the tensile hoop stresses. In reality, the actual tensile hoop stresses in the dome may be larger than the value presented above because of non-symmetrical or unexpected loadings on the dome, or extra loadings during construction. Thus, installation of steel ties is always a good practice in the design of masonry domes.

4.3 Steel ties

Steel ties were installed at the base of the dome above the arches top elevation (level 1) and at 4 different levels in the pendentives (levels 2-5), as shown in Figure 4.15. This configuration is the same at each of the 4 corners of the dome.

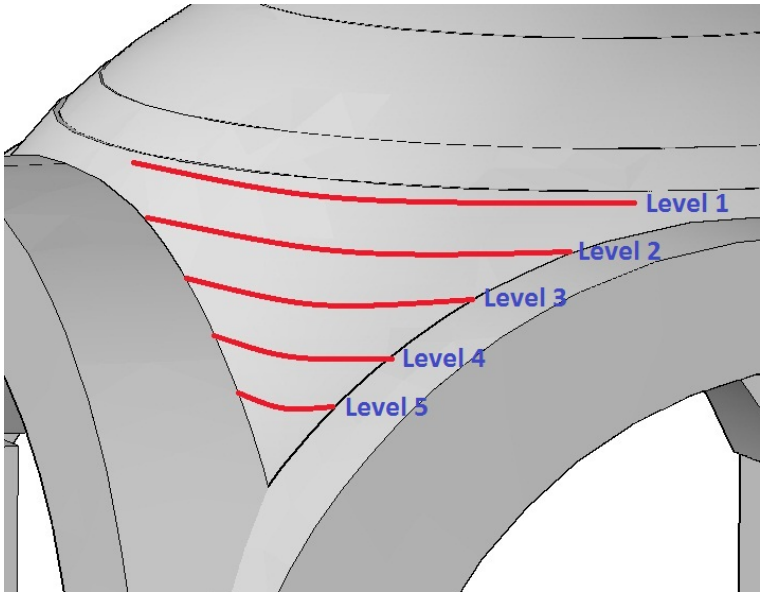

Figure 4.15: Steel ties location at one of the dome corners

All of the steel ties detailing have been obtained from the original architectural drawings of the structure, which were obtained from Avery Library Archives, Columbia University. One of the original drawings of the steel ties is presented in Appendix E. Table 4.4 shows all steel ties properties and details. The purpose of these steel ties is to help in resisting the tensile hoop forces acting at the lower sections of the dome. These steel ties are placed within the dome thickness, and their length vary between 14-25 *ft* depending on the level of the steel tie. [16]

The capacity of these tensile ties can be compared to the tensile hoop stresses shown in Table 4.3. The maximum hoop tensile stress from the table is 11,615 *lb*, and is almost half of the capacity of the steel ties in the pendentives. This implies that the capacity of steel ties are more than enough to carry the hoop tensile forces. On top of these steel ties, a tensile capacity is also provided by the confinement of the pendentives between the supporting arches towards the corners of the dome, and, if small, the tensile capacity of the

masonry dome itself. Combined, an effective tensile capacity with a high factor of safety is provided. This tensile capacity must be sufficient to carry unexpected or non-symmetric loadings.

Table 4.4: Steel ties properties and details

Level	Height above corner (ft)	Number of ties	Tie diameter (in)	Total area of ties (in^2)	f_y (ksi)	Tensile Capacity (lb)
1	30	6	0.75	2.65	55	145800
2	24	1	0.75	0.44	55	24200
3	18	1	0.75	0.44	55	24200
4	12	1	0.75	0.44	55	24200
5	6	1	0.75	0.44	55	24200

The most interesting aspect about these steel ties is the large amount of steel ties at the base of the dome (level 1). This level is at $\phi = 45°$ and is in the compressive hoop forces zone. This implies that, in theory, these steel are not necessary to be there as there are no tensile hoop stresses to resist. The stresses at this ϕ are confirmed to be compressive as shown in Table 4.3. Thus, this significant number of steel ties must be there for another purpose.

As was mentioned earlier in §1.3.2, this dome was constructed with no use of falsework or centering. This implies that the incomplete rings of the dome during construction should be sufficient to resist any tensile stresses that my develop due to their self-weight, any external falsework, and unpredictable loads during construction and at service. Guastavino Jr. was intuitive enough to realize that additional tensile stresses on the dome may occur due to several potential reasons, thus installed these steel ties to provide support and stability to the dome. But theoretically, the steel ties at the base of the dome (level 1) are in the compressive hoop stresses zone, and so unnecessary to be there when the completed dome is at service.

4.4 Non-symmetric loading

Non-symmetric loading conditions may occur often on such structures. These non-symmetric loadings may be due to wind, snow, or live loads. In this section, a lateral wind load of 30 lb/ft^2 will be imposed on the dome from one side, and the dome will be analyzed accordingly. Figure 4.16 shows this loading condition and the resulting vertical load on a cross-section of the dome. The analysis of non-symmetric loading will only be performed on the dome above the arches top elevation (i.e the cross dome section).

It is necessary to analyze non-symmetric loadings by taking a full cross-section of the dome rather than a cross-section of half the dome, as previously done. This is because a cross-section of half the dome with the self-weight and the imposed wind load is equivalent to a symmetric loading of a larger self-weight. Analyzing half a dome yields a thrust line that is symmetrical about the whole dome. This is not the case under non-symmetric loading. The cross dome lune section to be analyzed has the properties and dimensions as that analyzed under symmetric loading conditions. Here, there are two identical lunes opposite of each other and connected at the top, forming the full cross-section of the dome, as shown in Figure 4.16.

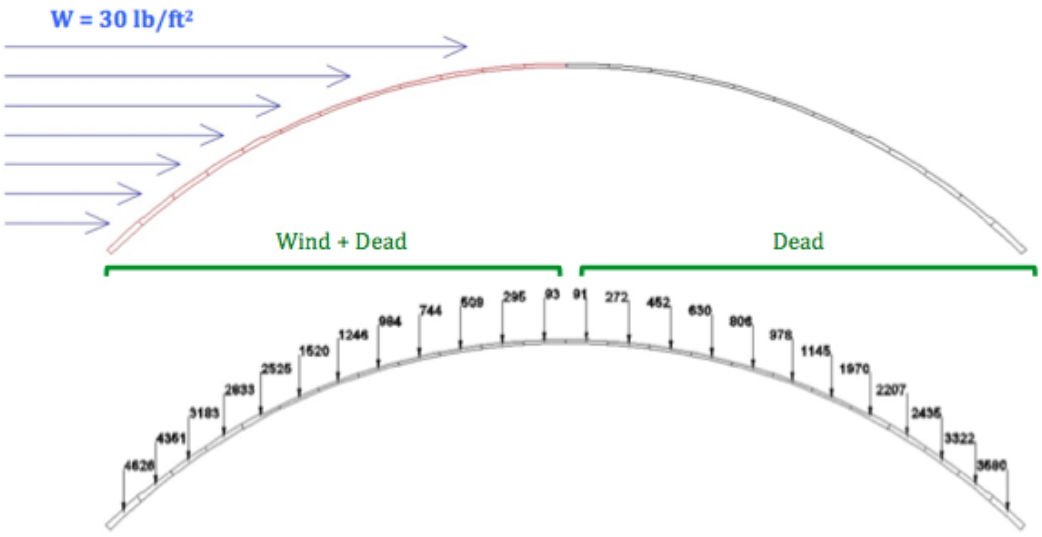

Figure 4.16: Non-symmetric loading condition and the resulting vertical loads on a full cross-section lune

4.4.1 Membrane analysis

Membrane analysis method cannot be used to analyze non-symmetric loading. This analysis method is only applicable for analyzing half cross-section lune of a dome. The calculations in this analysis cannot be expanded to analyze a full cross-section lune of a dome. Thus, analysis will be based on graphical methods and equilibrium equations.

4.4.2 Graphical analysis

Wolfe's graphical analysis methods cannot be used to analyze non-symmetric loading, for the same reason as that of the membrane analysis. However, the general approach of graphical methods can be applied to analyze non-symmetric loadings. The graphical analysis method that will be used to perform the analysis is the *funicular polygon method of thrust line analysis*. The methodology of this analysis method is presented in Appendix G. This method does not assume that the thrust line lies at the mid-thickness of the dome. The thrust line's slope depends on the vertical loading and the horizontal thrust on each section along the full lune. With these two orthogonal forces, the direction of the resultant thrust line at the centroid of each section of the full lune can be calculated. Consequently, the full thrust line profile can be determined.

Figure 4.17 shows the application of this analysis method on the full lune section and the resulting thrust line profile. It can be observed that the thrust line obtained using this analysis method does not lie within the thickness of the dome. The steps of this method were iterated multiple times to optimize the final thrust line profile, and Figure 4.17 shows this final optimized thrust line profile. This dome have resisted non-symmetric loading since its existence about 100 years ago. Thus, the obtained thrust line profile from this analysis method is not a representative of what is actually happening in the dome under non-symmetric loading. Another analysis technique will be used to determine the thrust line under non-symmetric loadings, and the results will be compared.

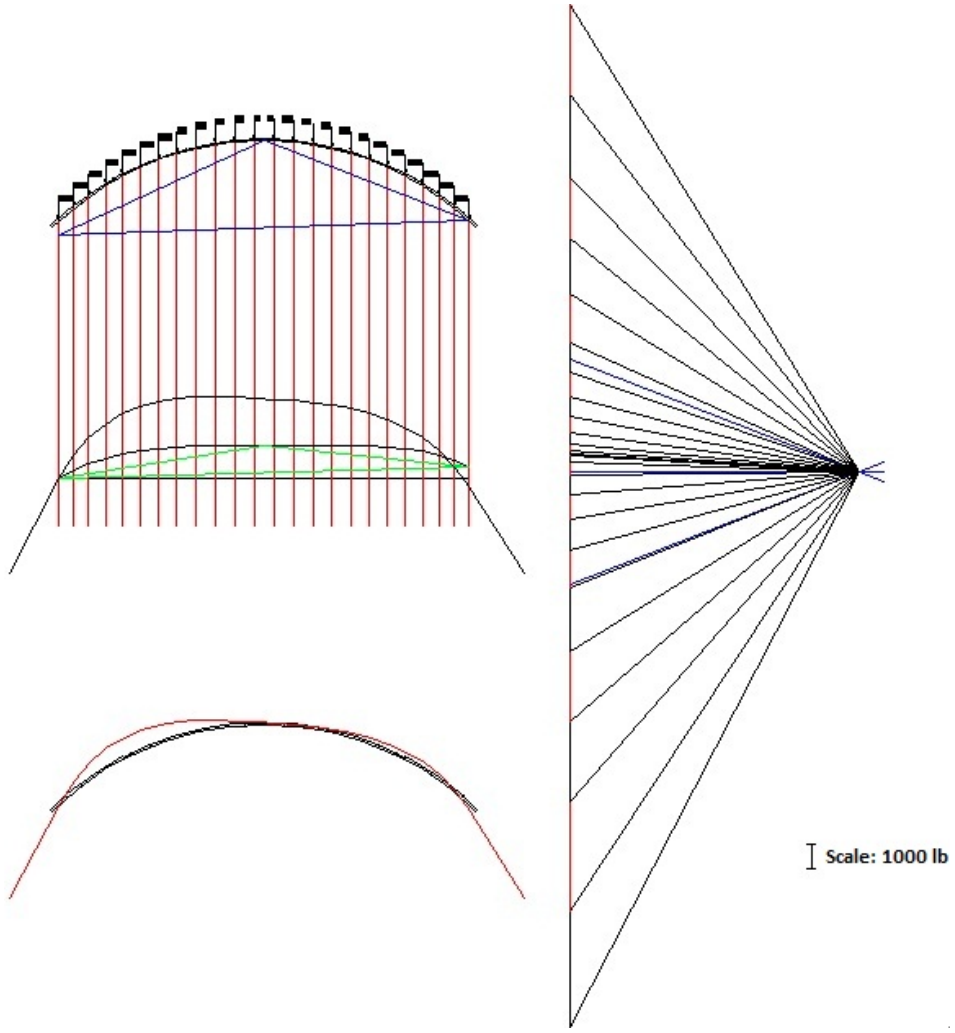

Figure 4.17: Funicular polygon analysis method (top left), the corresponding force polygon (right), and the imposed thrust line profile on the lune cross section (bottom left)

4.4.3 Analysis using equilibrium equations

The other method used to determine the thrust line profile is based on equilibrium equations. Figure 4.18 shows the overall concept of this calculation technique. The first step is to determine what are the support vertical reactions based on the applied vertical loads. The thrust line profile is determined segmentally starting on either of the supports. Based on the horizontal thrust and the vertical support reaction, one can determine what is the direction of the thrust line for the first section of the lune. The thrust line of the first section is extended until it reaches the vertical axis of the centroid of the second section of the lune. The net vertical load will decrease by the weight of this section, and the horizontal thrust remains the same. Based on these two forces, a new direction of the thrust line is determined, and is extended to the following section of the lune. This process is repeated until it goes over the full lune cross-section. This calculation can be done while keeping the horizontal thrust as a parameter. This parameter can then be varied to optimize the final thrust line profile. The most optimized thrust line profile of this method is shown in Figure 4.19.

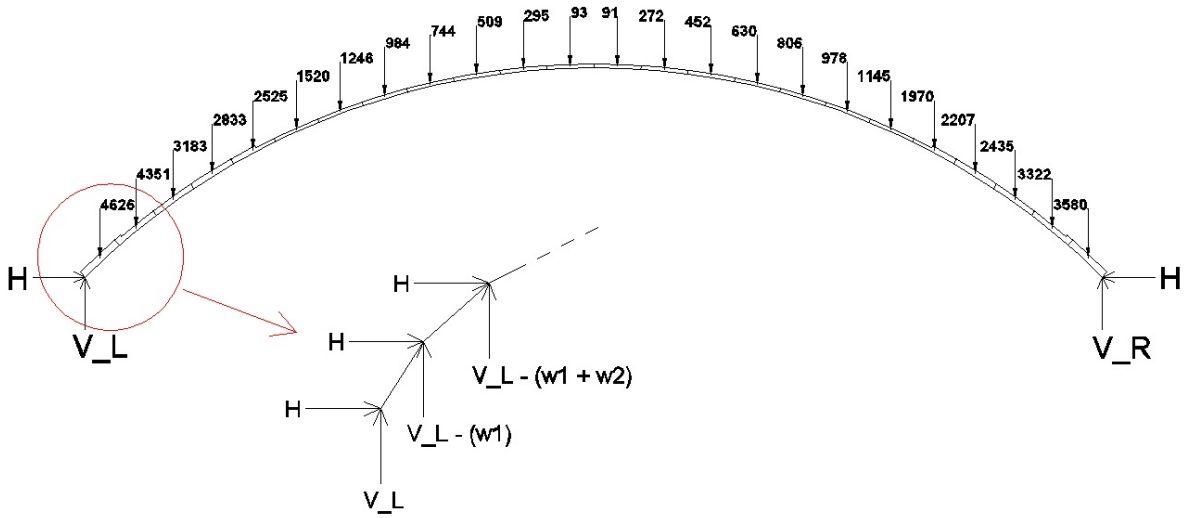

Figure 4.18: Thrust line calculations based on equilibrium equations

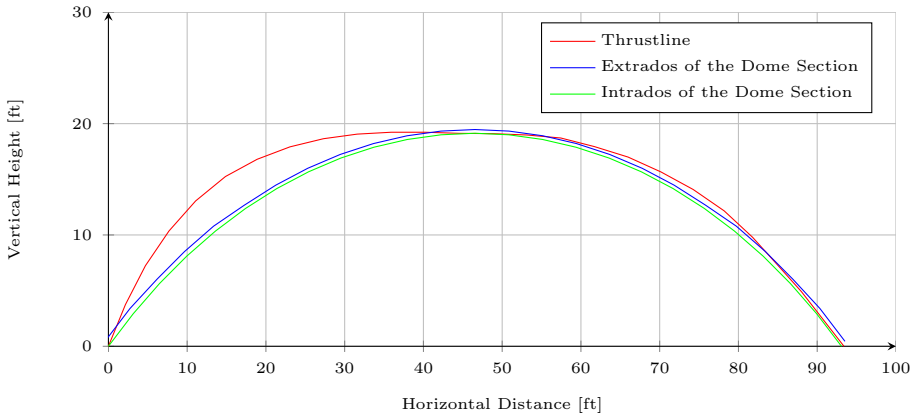

Figure 4.19: Thrust line profile of the full lune section determined using equilibrium equations

The result of this analysis method is similar to that of the graphical method. The thrust line profile obtained goes beyond the lune section thickness and implies that a thrust line within the dome cannot be obtained. This is the not the case in reality, thus different analysis techniques must be used to analyze this dome under non-symmetric loading conditions.

4.4.4 Discussion of the analysis results

The non-symmetric loading analysis using two different methods gave different results from the expected behaviour of this dome. Both analysis methods gave almost identical thrust line profiles, and the general shape of the thrust lines makes sense too. The general shape of the thrust line can be intuitively visualized if the full section is flipped upside down and thought of to be acting in pure tension. Since the non-symmetric loading induce higher vertical loadings on some sections of the lune, the thrust line tends to be attracted more to the higher loaded sections. Thus the general profile of the obtained thrust lines is correct. However, these thrust lines obtained are not confined within the dome's thickness and implies that the dome is

unstable under non-symmetric loading. This is not the case in reality, and so this type of analysis must be approached using other analysis techniques.

The conclusion from this analysis performed is that non-symmetric loading must be analyzed using the more in-depth 3D analysis methods. 2D analysis methods are known to give over-conservative results because of the assumptions and idealizations involved in their approach. Additionally, the 2D thrust line analysis methods neglect the effect of the hoop forces in pulling and maintaining the thrust lines within the thickness of the dome. As a result, the thrust lines obtained using 2D analysis methods that are not confined within the dome's section do not dictate that the more in-depth 3D analysis methods should give similar results.

4.5 Supporting arches

The dome is confined by the four great arches forming a square perimeter about the dome. The granite arches have a clear span of 85 ft and a 12x12 ft^2 cross-sectional surface. These arches are massive in size, and their relative size compared to the dome during construction can be seen in Figure 4.20. These arches carry the thrust coming from the dome and the pendentives, and transfer all the loads to the four main piers. The thrust line analysis of such a structural system have not been approached before. This section provides a strategy on how to calculate the thrust lines in such a case. The strategy is based on the fundamental principles of equilibrium methods.

Figure 4.20: One of the supporting arches during construction [3]

4.5.1 Analysis strategy

There are two challenging aspects when it comes to the analysis of such a loading condition and structural system. The first aspect is how to evaluate the horizontal thrust imposed from the dome and the pendentives on the arch; The dome exerts both meridional and hoop forces at the boundary between it and the arch, and these forces vary in magnitude along the boundary. The second aspect is how to actually determine the the resultant thrust line in the arch due to the combined loading of the thrust from the dome and the self-weight of the arch.

The first step is to evaluate the imposed thrust from the dome on the arch. As mentioned in the previous paragraph, these imposed forces consists of both the meridional and hoop forces coming from the dome. It is safe to disregard the hoop forces in this analysis, this is because the hoop forces are much lower than the meridional forces (as shown in Table 4.3). Additionally, the hoop forces are mostly resisted by the the steel ties within the dome and the pendentives, and so their significance on the arch is further reduced.

As for the meridional forces imposed from the dome on the arch. This force can be divided into its two horizontal and vertical components, as shown in Figure 4.21. The vertical component is also disregarded as it is much smaller compared to the self-weight of the arch. For example, the vertical component of the meridional force at the boundary of the cross lune is 17,798 *lb* (this value is calculated using the *M Support* and *M Horizontal* values of the cross lune from Table 4.3), and the self-weight of the arch segment at that point is 253,344 *lb* (an order of magnitude larger). Thus, it is safe to disregard the vertical component of the meridional forces in this analysis

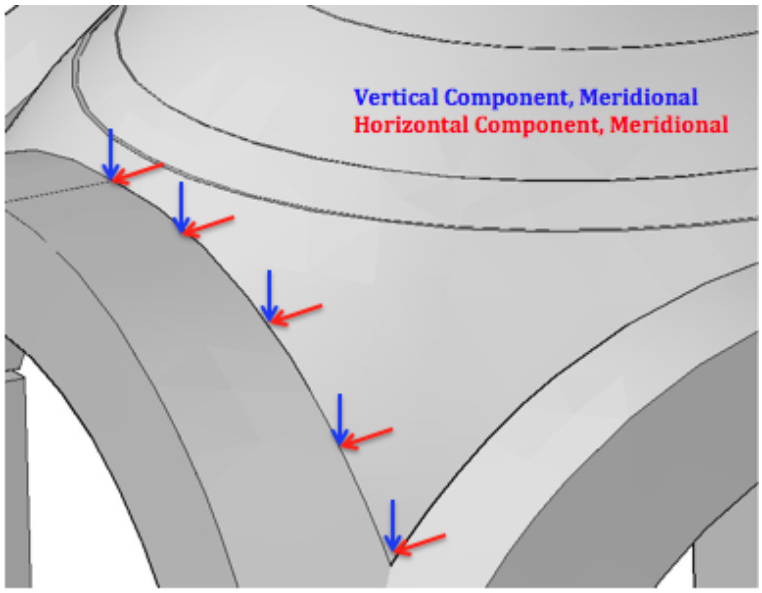

Figure 4.21: Components of the meridional forces of the dome on the supporting arch

With these assumptions, the imposed loads from the dome on the arch are the horizontal components of the meridional forces only. This horizontal component varies along the boundary between the dome and the supporting arch. It is assumed that this horizontal force varies linearly from the top mid-point of the arch

(where the cross lune section of the dome meets the arch) to the ends of the arch (where the diagonal lune section of the dome meets the arch). With this assumption, and knowing what are the horizontal component of the meridional forces at these two points, the applied horizontal forces along the boundary with the arch can be determined.

The arch has been divided into nine identical sections. The self-weight and the centroid of each section have been determined accordingly. The horizontal forces from the dome have been calculated according to the width of the arch sections and are applied on the centroid of each section of the arch. The self-weight of the arch sections are applied at the centroid too. Figure 4.22 shows the the loads applied on the arch sections.

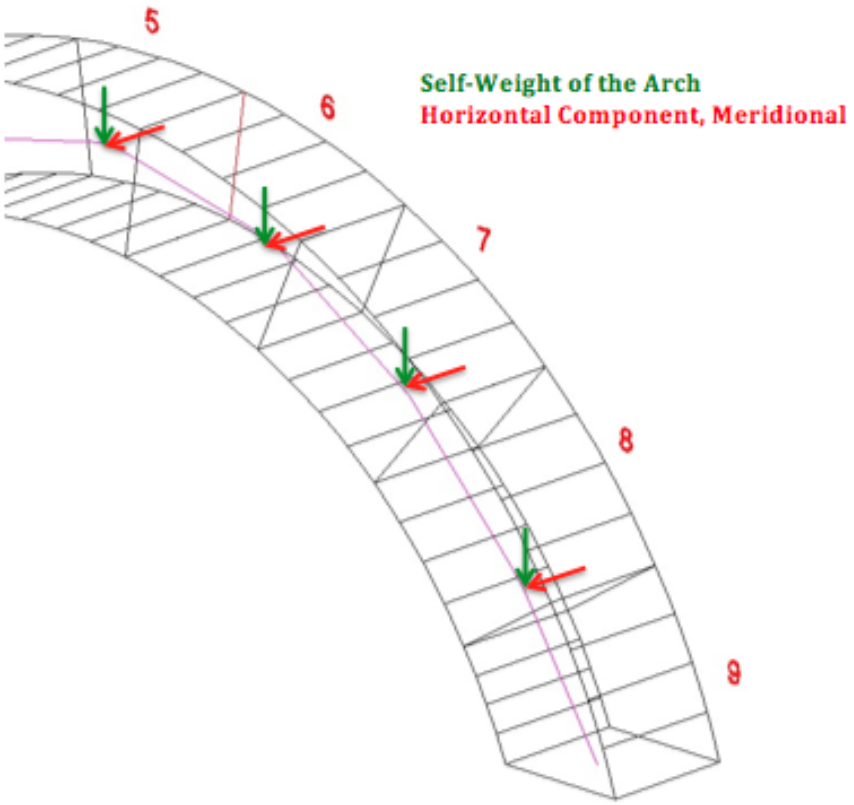

Figure 4.22: Final horizontal and vertical loads applied on the supporting arches

Now that the loads are figured out, the analysis of the arch can be determined. Membrane and Wolfe's graphical analysis methods cannot be applied on this arch, as they analyze only a half cross-section of an arch. The horizontal forces acting on the arch make these methods inapplicable too. The graphical method that will be used is the *funicular polygon method of thrust line analysis*, which is the same method used for the analysis of the dome under non-symmetric loading. This method is capable of determining a thrust line for the full arch under vertical loads, however, it can be expanded to an extra dimension to include the horizontal force components acting on the arch. First, this method is used to determine a thrust line for the arch under self-weight only, as shown in Figure 4.23. The weight of each section of the arch was calculated to be 253,344 *lb* acting on the centroid of each section, and the total thrust, F, was determined to be 1,549,592 *lb* acting in the direction shown in Figure 4.23.

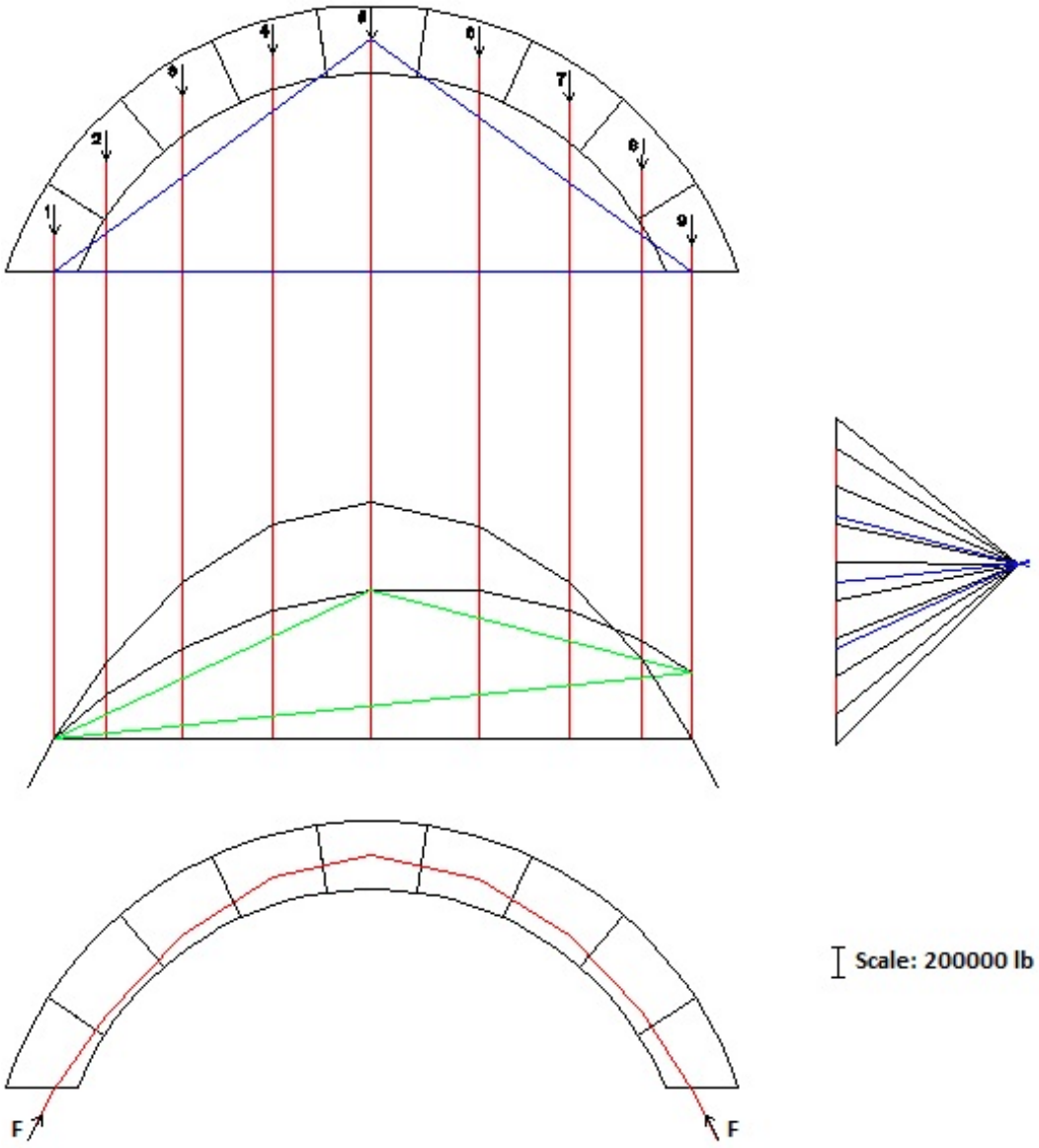

Figure 4.23: Funicular polygon analysis method (top left), the corresponding force polygon (right), and the imposed thrust line on the arch (bottom left)

A possible thrust line that lies within the thickness of the arch under self-weight only is determined. This thrust line is assumed to be acting at the centerline of the arch (along the mid-width of the arch). The horizontal forces acting on the arch will push the thrust line away from the centerline, cumulatively from the top mid-point and towards the two ends of the arch. The length by which the thrust line is pushed horizontally is the horizontal force at each section of the arch multiplied by the same scale used on the self-weight load throughout the funicular polygon analysis method. Figures 4.24 and 4.25 show a plan view and an isometric view of the final thrust line within the arch. Please note that the loads in Figure 4.24 are actually acting on the centroid of each of the arch sections, but are displayed this way to better show the thrust line within the arch.

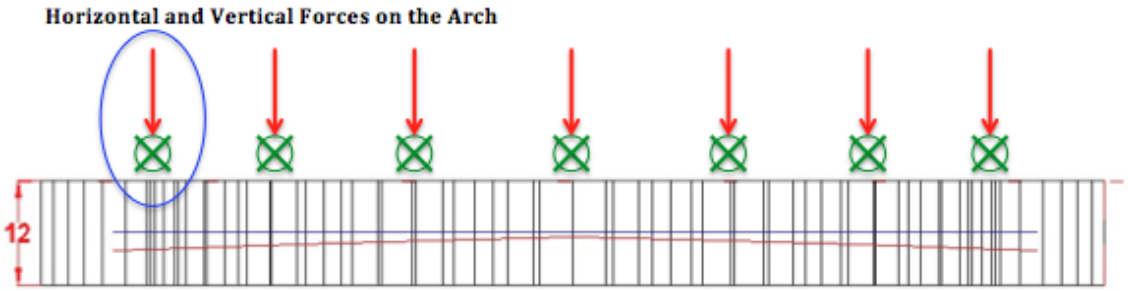

Figure 4.24: Plan view of the final thrust line within the supporting arch

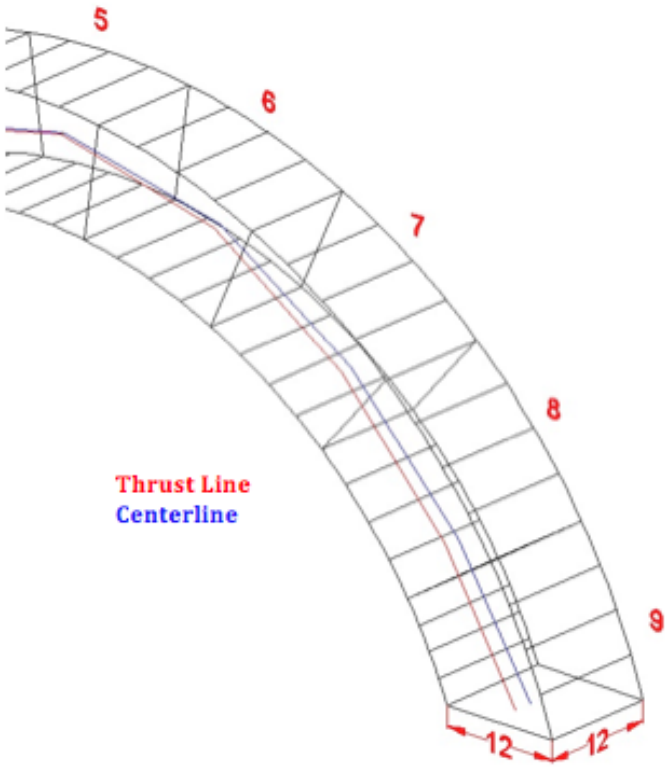

Figure 4.25: Isometric view of the final thrust line within the supporting arch

4.5.2 Discussion of the analysis results

The three main assumptions used in this strategy are:

- Disregard the hoop forces from the dome and the pendentives, as they are much smaller relative to the meridional forces
- Disregard the vertical component of the meridional forces, as they are much smaller relative to the self-weight of the arch
- The horizontal component of the meridional forces, from the dome and the pendentives, varies linearly from the top and towards the two ends of the arch.

With these assumptions, a thrust line for the supporting arches can be determined.The thrust line lies completely within the arch and the total horizontal displacement of the thrust line from the centerline of the arch was calculated to be 1.87 *ft*. This implies that the thrust line lies within the middle third of the width of the arch, and that the supporting arches have a reasonable safety factor, which, in a matter of fact, can be calculated.

A parametric study can be done to evaluate what is the critical width necessary for the arch to carry the horizontal thrust from the dome as well as its self-weight. The parameter in this study is the width of the arch, and all the other variables, such as the horizontal loads from the dome, and the other two dimensions of the arch, are kept the same. One can vary the width of the arch, and the modified total horizontal displacement of the thrust line can be determined accordingly. Using trial and error, the critical width of the arch can be determined. Note that once the width of the arch is reduced, the mass is reduced, so the proportional significance of the horizontal forces compared to vertical self-weight loads *increases*. This implies that the relation between the width of the arch and the total horizontal displacement of thrust line is *not* linear. With that, the critical width of the arch is calculated to be around 6.7 *ft*. The total horizontal displacement of the thrust line is 3.35 *ft* in this case (assuming the thrust line is originally at the centerline of the arch). With this critical width, the safety factor of the arch is *12/6.7*, or 1.8.

The strategy proposed to analyze the thrust lines in the four great arches provided satisfactory results. The resulted thrust line lies within the middle third of the arch and has a safety factor of 1.8.

This section concludes the various analyses performed on the dome of the Cathedral of Saint John the Divine and its supporting arches. The main conclusions of this thesis and possible areas of future work are presented in the following section.

5 Conclusions

5.1 Summary of Results

This thesis provided an insight into the history and behaviour of the Guastavino masonry dome of the Cathedral of Saint John the Divine. A complete quantitative and qualitative analysis has been performed and the main results are summarized as follows:

- 2D equilibrium methods are suitable to analyze the forces in masonry domes. These methods analyze the forces in a lune section of a dome, and the results of this lune are representative of the complete dome. The equilibrium methods used were membrane and graphical analysis methods, and the results of both analysis methods are consistent with each other.
- 2D equilibrium methods have been used to determine the meridional and hoop forces within the dome under its self-weight, and evaluate a possible thrust line within the thickness of the dome. The calculated forces are an order of magnitude less than the strength capacity of the masonry tiles. This proves that the stability of the dome is indeed a question of geometry rather than strength.
- In the case of non-symmetric loading conditions on the dome, the 2D equilibrium methods did not evaluate thrust lines within the thickness of the dome. This implies that the hoop forces acting radially about the dome are necessary to pull back and maintain the thrust lines within the thickness of the dome. Thus, it is necessary to apply in-depth 3D analysis methods in the case of non-symmetric loading, to better evaluate the thrust lines. A possible method is the thrust network analysis method developed by Philippe Block. [17] The application of 3D equilibrium methods are beyond the scope of this thesis.
- Steel ties exist at four different levels within the pendentives, and at one level at the base of the dome. The steel ties in the pendentives are necessary to take on the tensile hoop forces. The steel ties at the bottom of the dome exist in the compressive hoop forces zone, and theoretically, they are not necessary to be there. However, there exist several potential reasons that may cause additional tensile stresses on the dome during construction and at service. Thus, these steel ties provide additional stability and safety to the dome.
- This thesis presented a strategy on how to evaluate the thrust lines in the great arches supporting the dome. The flow of forces is complicated at the boundary between the dome and the arches, and three main assumptions were necessary to idealize the system and obtain a thrust line within the arches. The resulted thrust line lies within the middle third of the arch width, and this implies that the arch is within good safety limits. The factor of safety of the arch has been calculated to be 1.8.

5.2 Future Work

The analysis of this dome revealed many interesting results, but also motivates for areas of further research:

- The performed analysis determined possible thrust lines under specific loading conditions, one proposal for future work is to find upper bound solutions, that is, the loading conditions leading to the collapse of the dome
- It was concluded that 2D analysis methods are not sufficient to analyze the structure under non-symmetric loading. Another proposal is to use 3D analysis methods to analyze the structure under this loading scenario, possibly by the thrust network analysis method developed by Philippe Block. [17]
- This thesis provided a strategy to analyze the flow of forces of the supporting arches of the dome. A future work would be to further expand this approach, and better idealize the structure in terms of loads magnitude and location.

As a final reflection, this thesis paper presented a well-rounded analysis assessment of one of the most fascinating masonry domes in the world. The incredible thinness of this dome relative to its span and the courageous construction technique imply that the Guastavinos had a deep instinct and grasp of the design and construction of masonry structures.

References

[1] Quirk, Howard (1993). *The living cathedral: St. John the Divine: A history and guide*. New York: The Crossroad Publishing.

[2] Ochsendorf, John (2010). *Guastavino vaulting: The art of structural tile*. New York: Princeton Architectural Press.

[3] Cathedral Images (1909). Archives Department, Episcopal Diocese of New York. New York. Retrieved on March 7, 2013.

[4] Anonymous (1909a). *Progress of construction of the Cathedral of Saint John the Divine*. The Engineering Record, Vol. 59, No. 4. New York: McGraw Publishing.

[5] Anonymous (1909b). *Erecting a large dome without falsework*. The Engineering Record, Vol. 60, No. 19. New York: McGraw Publishing.

[6] Allis, Sam (2011). *The greatest architect you've never heard of*. www.boston.com. Accessed on April 13, 2013.

[7] Heyman, Jacques (1995). *The stone skeleton: Structural engineering of masonry architecture*. Cambridge: Cambridge University Press.

[8] Dreyfuss, Miryam (2011). *Limit Analysis of the great hall of Trajan's Markets in Rome using equilibrium methods*. Master's Thesis. Massachusetts Institute of Technology

[9] Zessin, Jennifer (2012). *Collapse analysis of unreinforced masonry domes and curving walls*. PhD dissertation. Massachusetts Institute of Technology.

[10] Lau, Wanda (2006). *Equilibrium analysis of masonry domes*. Master's thesis. Massachusetts Institute of Technoogy.

[11] Wolfe, William (1921). *Graphical analysis: A textbook on graphic statics*. New York: McGraw-Hill.

[12] Reese, Megan (2008). *Structural analysis and assessment of Guastavino vaulting*. Master's thesis. Massachusetts Institute of Technology.

[13] Guastavino, Rafael (1893). *Essay on the theory and history of cohesive construction, applied especial to the timbrel vault*. Boston: Ticknor.

[14] Huerta, Santiago (2003). *Mechanics of masonry vaults: Ahistorical outline: Essays on the history of mechanics*. In A. Becchi, M. Corradi, F. Foce, and O. Pedemonte (Eds.). Basel: Birkhäuser.

[15] Atamturktur, Huriye Sezer (2006). *Structural assessment of Guastavino domes*. Master's thesis. Pennsylvania State University.

[16] Original Guastavino Drawings (1909). Drawings & Archives Department, Avery Architectural & Fine Arts Library, Columbia University. New York. Retrieved on March 7, 2013.

[17] Block, Philippe (2009). *Thrust network analysis: Exploring three-dimensional equilibrium*. PhD dissertation. Massachusetts Institute of Technology.

Appendices

A Derivation of the point of zero hoop stress for a dome

At zero hoop stresses, N_θ from Equation 2.2 is set to zero, and then the equations is simplified to calculate the value of θ.

$$N_\theta = wa\ (\frac{1}{1+\cos(\phi)} - \cos(\phi)) \tag{A.1}$$

$$0 = wa\ (\frac{1}{1+\cos(\phi)} - \cos(\phi)) \tag{A.2}$$

$$0 = \frac{1}{1+\cos(\phi)} - \cos(\phi) \tag{A.3}$$

$$1 = \cos(\phi) + \cos^2(\phi) \tag{A.4}$$

Solving for ϕ from Equation A.4 will yield an answer of $51.82°$.

B Section properties of the generic dome lune

Section 1 is at the crown of the lune, and section 10 is at the base of the lune.

Table B.1: Section properties of the generic dome lune

Section	ρ (pcf)	θ (°)	ϕ_1 (°)	ϕ_2 (°)	R_o (ft)	R_i (ft)	V (ft^3)	w (lb)
1	112.00	15.00	0.00	7.00	65.17	64.83	2.75	308.40
2	112.00	15.00	7.00	14.00	65.17	64.83	8.22	920.62
3	112.00	15.00	14.00	21.00	65.17	64.83	13.56	1519.10
4	112.00	15.00	21.00	28.00	65.17	64.83	18.70	2094.95
5	112.00	15.00	28.00	35.00	65.17	64.83	23.57	2639.56
6	112.00	15.00	35.00	42.00	65.17	64.83	28.08	3144.83
7	112.00	15.00	42.00	49.00	65.17	64.83	32.17	3603.21
8	112.00	15.00	49.00	56.00	65.17	64.83	35.78	4007.89
9	112.00	15.00	56.00	63.00	65.17	64.83	38.86	4352.81
10	112.00	15.00	63.00	70.00	65.17	64.83	41.36	4632.85

C Wolfe's analysis method assuming tensile capacity for the dome

The methodology presented here is reproduced from Megan Reese thesis. [12]

Wolfe's graphical analysis method assuming tensile capacity for the dome is explained here in greater detail. The figures referred to are given on the pages following the explanation. Each figure depicts a cross-section of the lune on the left side of the figure and the force polygon on the right side. Each line of the force polygon represents an internal or external force acting on or within the lune. The orientation of each line in the force polygon is the same as that of the force on or within the lune. The length of each line in the force polygon corresponds to the magnitude of each force.

- Figure (a). Apply the ten lune segment weights as point loads to the lune cross-section. Draw ten vertical line segments to a scale representing each load, and connect them end to end. This line is called the "load line," and it represents the start of the force polygon. Draw a horizontal line at the top of the load line, extending to the right. This line will be used to represent the horizontal forces in the system, and its length will be determined later. This horizontal line corresponds to the first segment of the "thrust line" at the crown of the lune cross-section. The thrust line represents one set of internal forces within the lune - the meridional forces.
- Figure (b). The next step is to approximate the thrust line within the dome using the assumption from membrane theory that the forces are restrained to the mid-surface layer of the dome thickness. Draw a line connecting the centers of the top two segments of the lune. Maintaining the orientation of this line, copy it to the force polygon so that it starts between the load line segments of the top two segments. End the line wherever it intersects with the horizontal line. The length of this line in the force polygon approximates the meridional force in that region of the lune. Drawing this first meridional force also determines the magnitude of the horizontal force acting at the crown of the lune.
- Figure (c). Repeat the last step, drawing the next segment of the thrust line to determine the next meridional force.
- Figure (d). Repeat eight more times. The inclusion of tensile capacity allows the thrust line to "turn downwards" and follow the non-funicular form of the hemisphere. The last segment of the thrust line is parallel to the reaction at the base of the lune, so this reaction is of the same magnitude as the last segment of the force polygon. The length of the horizontal line drawn in Figure (c) is determined by its furthest right intersection with a meridional force on the force polygon.
- Figure (e). A plan-view of the lune has been added to the remaining figures above the lune cross-section. Two forces are drawn perpendicular to the edge of the lune pointing towards the center of the first lune segment. Since these forces are pushing on the lune, they are compressive forces. Maintaining the orientation of these lines, copy them to the force polygon as shown. These segments will represent the other set of internal forces for the lune - the hoop forces.
- Figure (f). Repeat the last step to find the next hoop force.

- Figure (g). Repeat five more times to find the magnitudes of the compressive hoop forces. This brings one to the right end of the horizontal line. The same process will be repeated to find the tensile hoop forces, now working from right to left below the horizontal line.
- Note that one lune segment does not have a hoop force. This is because the two points that would be used to determine that hoop force on the force polygon are very close to each other, thus the hoop force lines would be so short to be practically zero.
- Figure (h). Using the same methodology as for the hoop forces, draw two forces at the base of the lune plan view perpendicular to the edges of the lune. Maintaining the orientation of these lines, "close" the force polygon by connecting one line to the end of the last tensile hoop force line and the other to the left end of the horizontal line. These force represent the required force in the tension tie to carry the thrust of the dome.

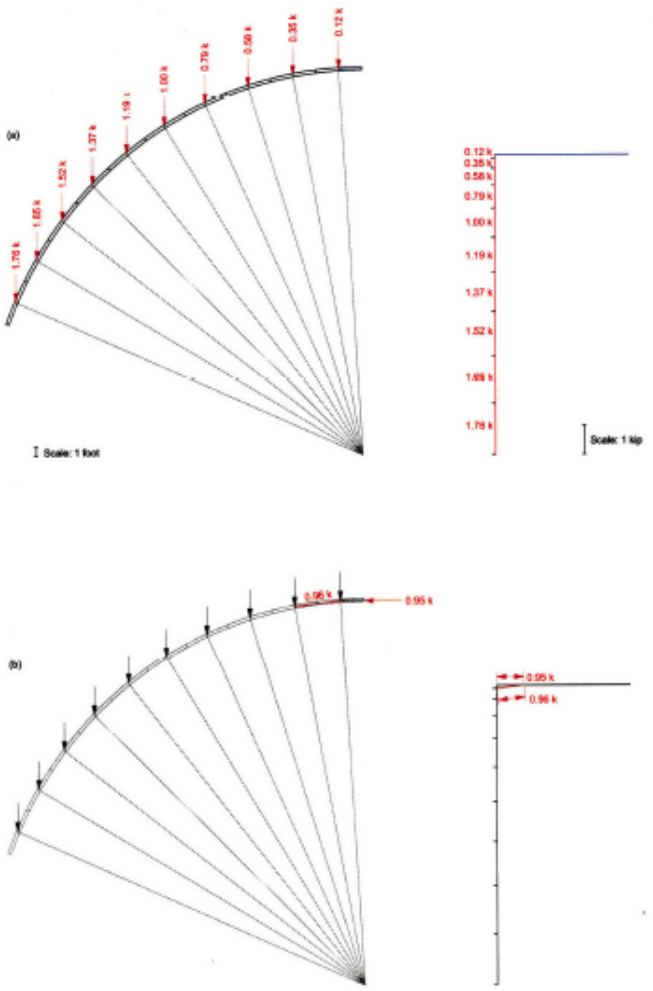

Figure C.1: Figures (a) and (b) [12]

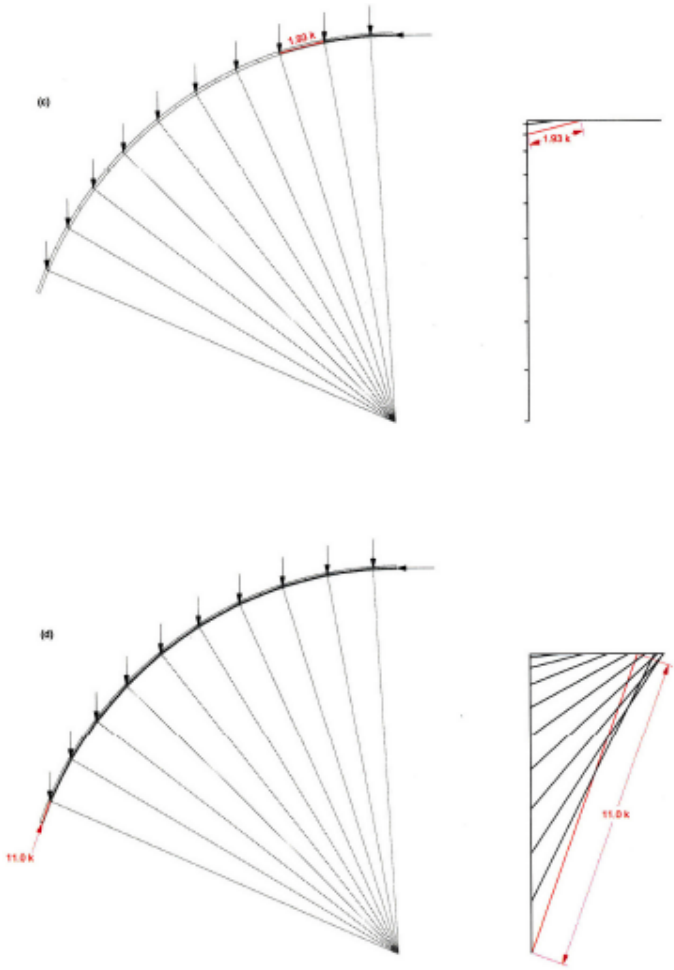

Figure C.2: Figures (c) and (d) [12]

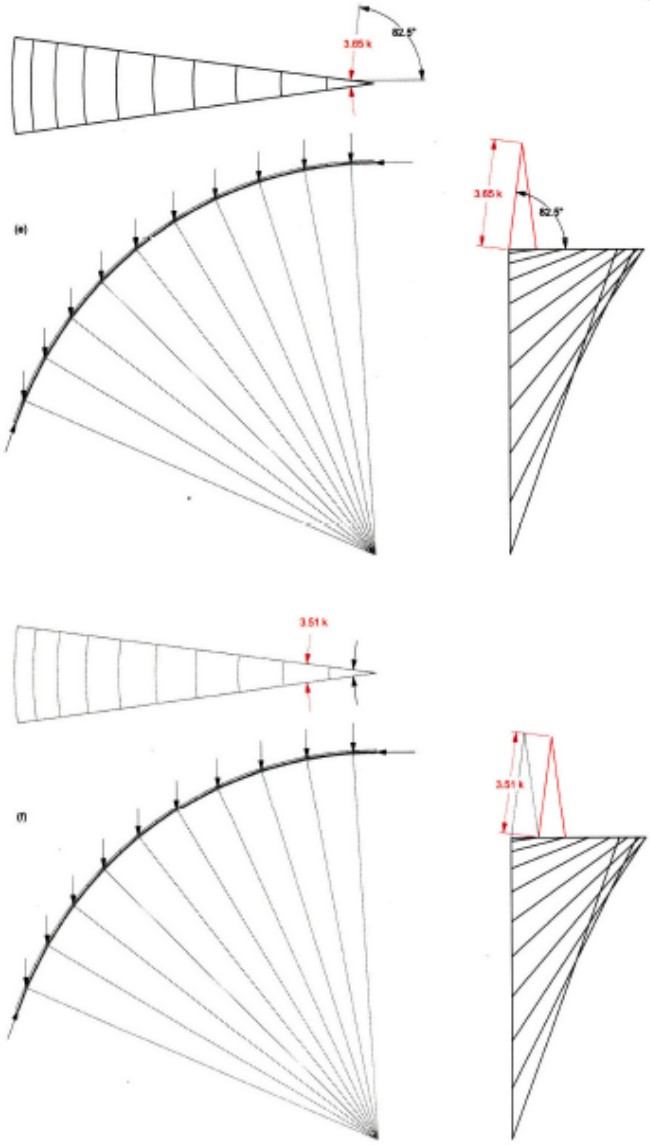

Figure C.3: Figures (e) and (f) [12]

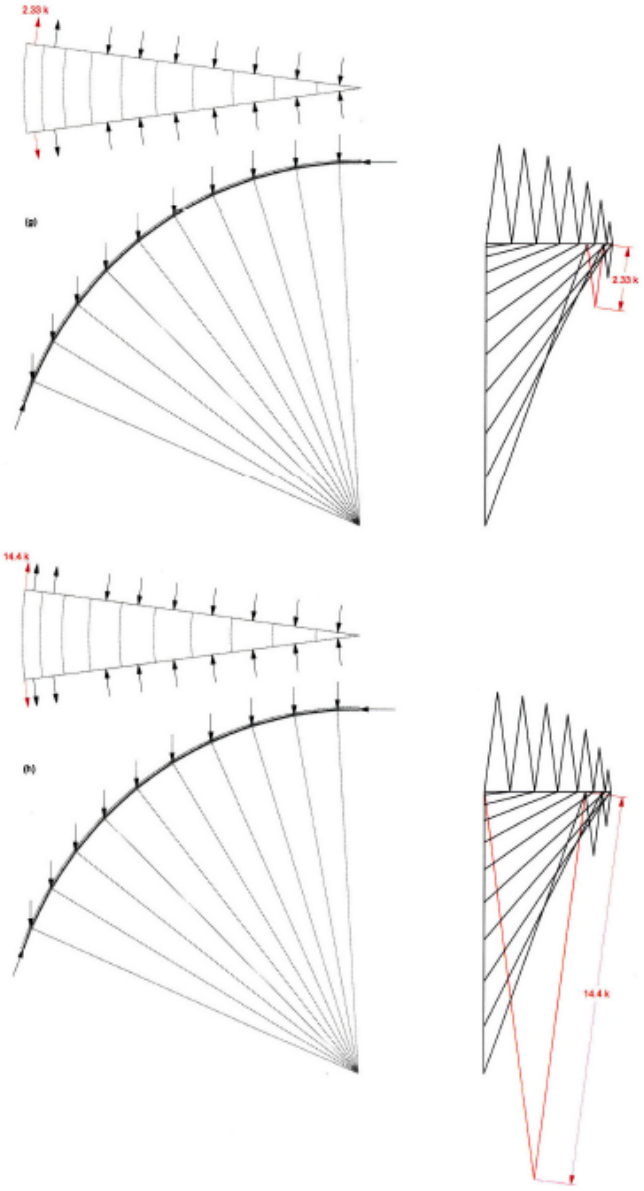

Figure C.4: Figures (g) and (h) [12]

D Wolfe's analysis method assuming no tensile capacity for the dome

The methodology presented here is reproduced from Megan Reese thesis. [12]

Guastavino domes were built with steel reinforcing or buttressing that provides support for a dome in the region of tensile hoop forces ($\phi > 51.82°$). If steel tensile reinforcing within the dome material has rusted or if the buttressing is insufficient, it is possible to analyze the dome using the second graphical method for a dome without tensile capacity introduced by Wolfe [11] to evaluate its stability. The methodology is essentially the same as that described in Appendix C, except that there are no tensile hoop forces to restrain the thrust line to the centerline of the dome thickness for $\phi > 51.82°$. In Figure 2.6, the right half of Wolfe's Fig. 500 shows that the thrust line for the dome without tensile capacity does not have the same spherical shape below line Y_1-Y_1 as the thrust line on the left half of Fig. 500.

The analysis begins by constructing the load line and drawing the horizontal line in the exactly the same way as was done in Figure (a) of Appendix C. Next, the thrust line is drawn within the dome thickness in the region of $0° < \phi < 51.82°$ following the methodology illustrated in Figures (b) through (d) of Appendix C, and these lines are transferred to the force polygon as before. The thrust line and force polygon at this stage is given in Figure D.1.

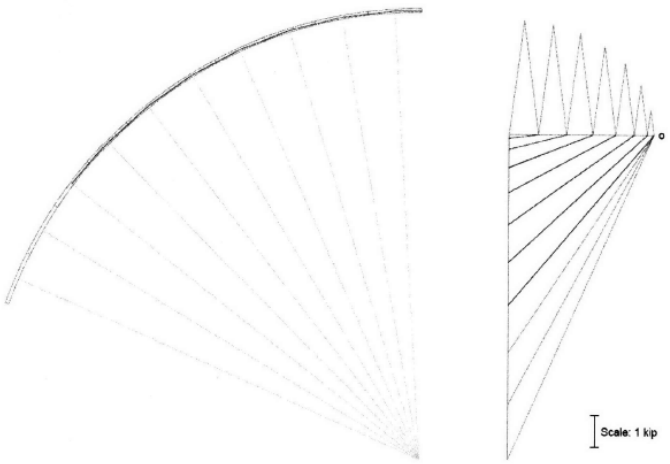

Figure D.1: Thrust line (left) and force polygon for dome in the region $0° < \phi < 51.82°$ [12]

Constructing the rest of the thrust line deviates from the method in Appendix C at this point. To complete the thrust line, line segments are drawn first on the force polygon, starting at the point labeled 'o' in Figure D.1 and ending between the load line segments. While maintaining the same orientation, these line segments are copied to the thrust line. The hoop forces are then determined in the region of $0° < \phi < 51.82°$ in the same manner as described by Figures (e) through (g) of Appendix C. There are no hoop forces in the part of the dome where $\phi > 51.82°$.

E Original drawings of the dome of the cathedral

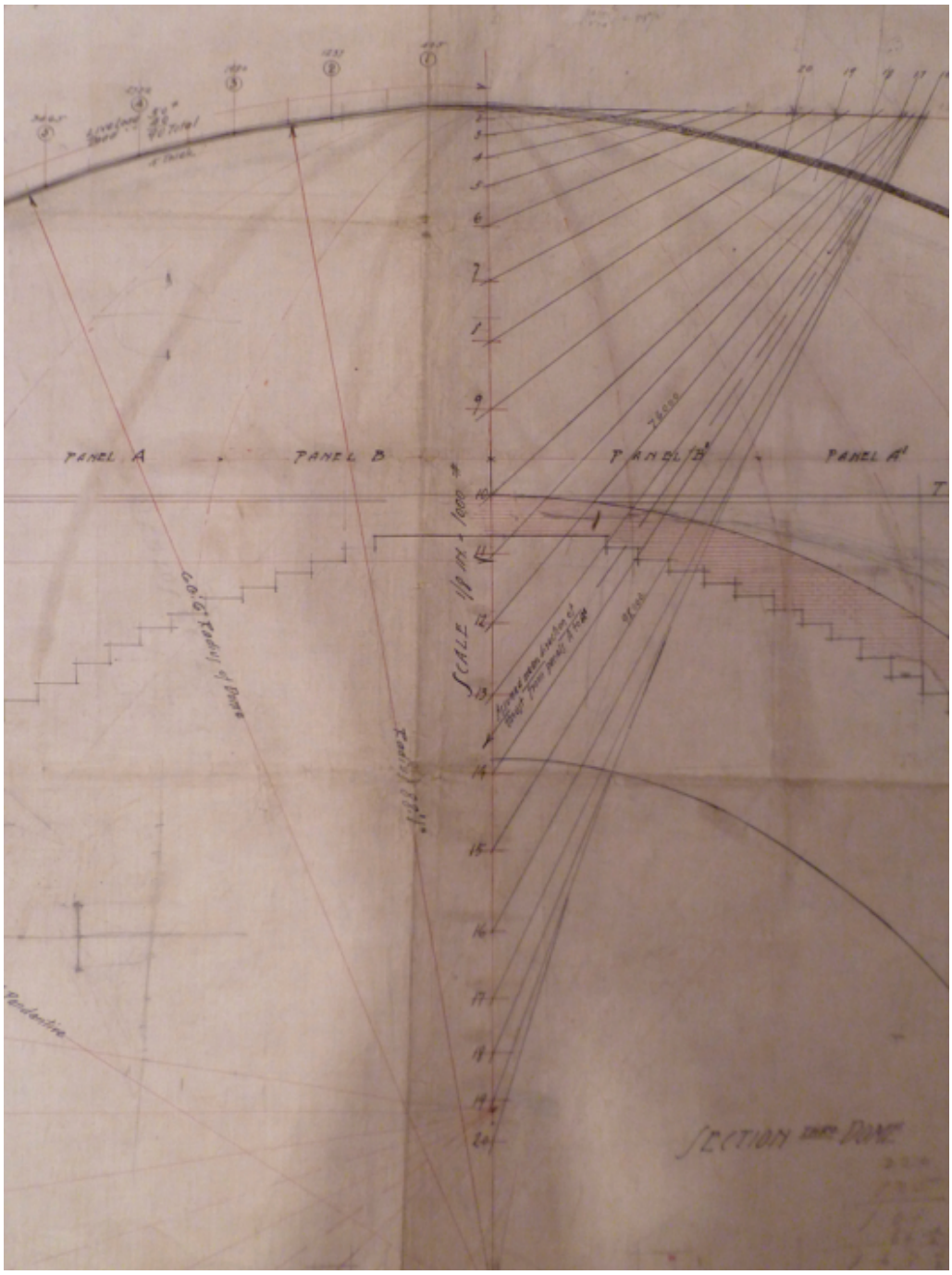

Figure E.1: Original drawing showing graphical analysis performed on the dome [16]

Figure E.2: Original drawing showing the details of the tiles [16]

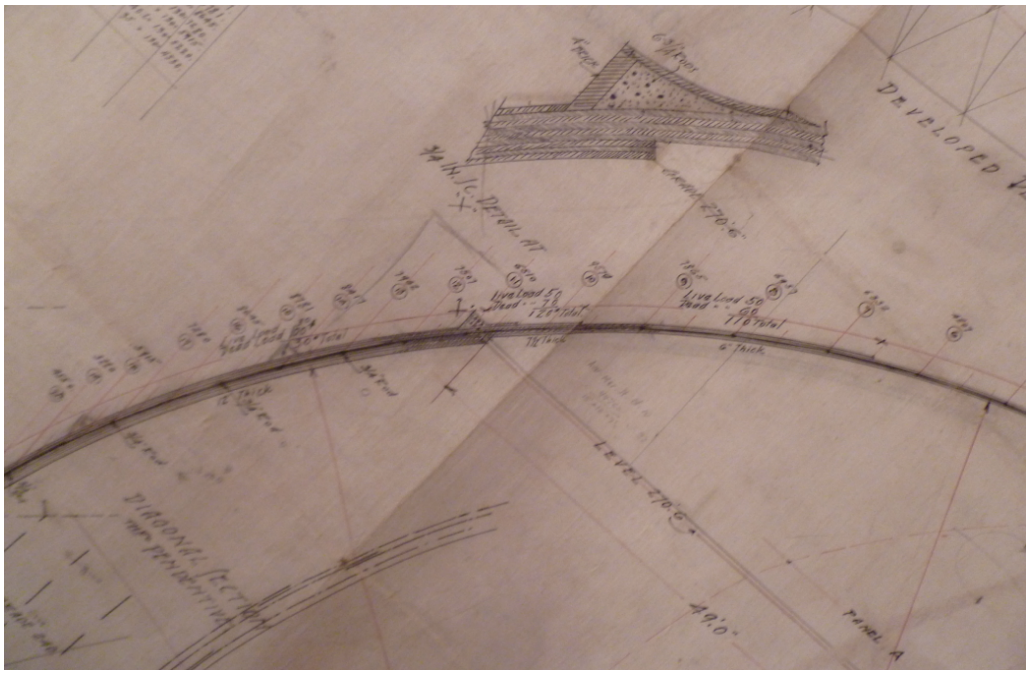

Figure E.3: Original drawing showing more details of the tiles and the steel ties [16]

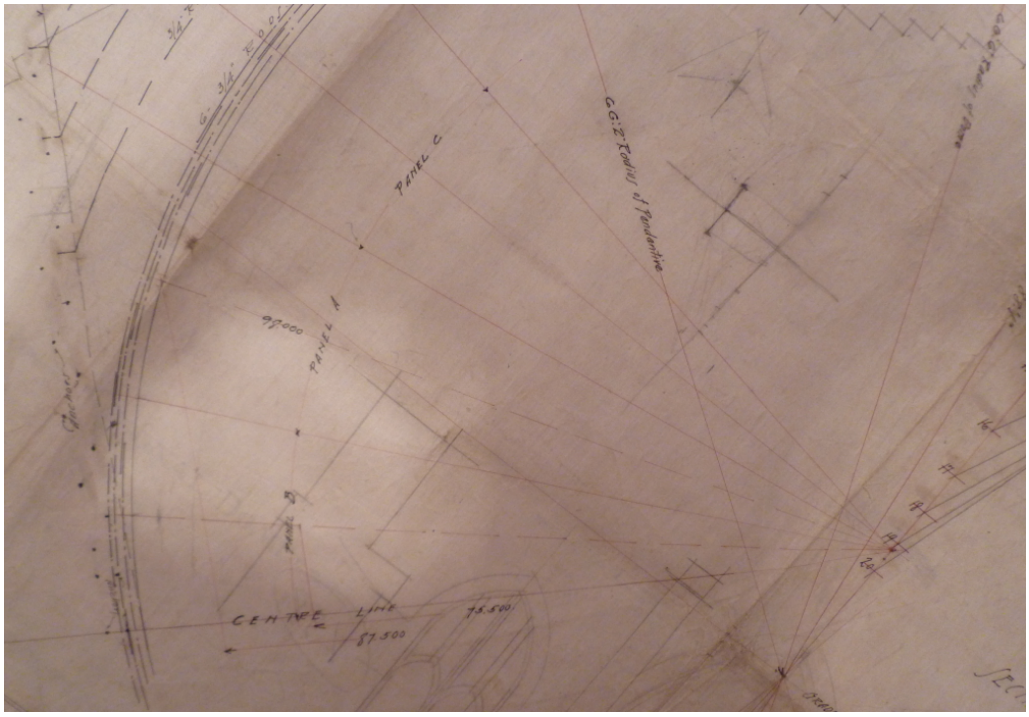

Figure E.4: Original drawing showing the general geometry of the dome [16]

F Section properties of the dome of the cathedral

F.1 Cross Lune

Section 1 is at the crown of the lune, and section 12 is at the base of the lune.

Table F.1: Section properties of the cross dome lune

Section	ρ (pcf)	θ (°)	ϕ_1 (°)	ϕ_2 (°)	R_o (ft)	R_i (ft)	V (ft^3)	w (lb)
1	112.00	15.00	0.00	3.80	66.50	66.17	0.81	90.77
2	112.00	15.00	3.80	7.50	66.50	66.17	2.43	271.94
3	112.00	15.00	7.50	11.30	66.50	66.17	4.04	451.95
4	112.00	15.00	11.30	15.00	66.50	66.17	5.63	630.06
5	112.00	15.00	15.00	18.80	66.50	66.17	7.19	805.50
6	112.00	15.00	18.80	22.50	66.50	66.17	8.73	977.54
7	112.00	15.00	22.50	26.30	66.50	66.17	10.23	1145.45
8	112.00	15.00	26.30	30.00	66.67	66.17	17.59	1969.71
9	112.00	15.00	30.00	33.80	66.67	66.17	19.70	2206.85
10	112.00	15.00	33.80	37.50	66.67	66.17	21.74	2434.67
11	112.00	15.00	37.50	41.30	66.80	66.17	29.66	3321.51
12	112.00	15.00	41.30	45.00	66.80	66.17	31.96	3579.90

F.2 Diagonal Lune

Section 1 is at the crown of the lune, and section 21 is at the base of the lune.

Table F.2: Section properties of the diagonal dome lune

Section	ρ (pcf)	θ (°)	ϕ_1 (°)	ϕ_2 (°)	R_o (ft)	R_i (ft)	V (ft^3)	w (lb)
1	112.00	15.00	0.00	3.80	66.50	66.17	0.81	90.77
2	112.00	15.00	3.80	7.50	66.50	66.17	2.43	271.94
3	112.00	15.00	7.50	11.30	66.50	66.17	4.04	451.95
4	112.00	15.00	11.30	15.00	66.50	66.17	5.63	630.06
5	112.00	15.00	15.00	18.80	66.50	66.17	7.19	805.50
6	112.00	15.00	18.80	22.50	66.50	66.17	8.73	977.54
7	112.00	15.00	22.50	26.30	66.50	66.17	10.23	1145.45
8	112.00	15.00	26.30	30.00	66.67	66.17	17.59	1969.71
9	112.00	15.00	30.00	33.80	66.67	66.17	19.70	2206.85
10	112.00	15.00	33.80	37.50	66.67	66.17	21.74	2434.67
11	112.00	15.00	37.50	41.30	66.80	66.17	29.66	3321.51
12	112.00	15.00	41.30	45.00	66.80	66.17	31.96	3579.90
13	112.00	15.00	45.00	48.80	67.17	66.17	54.93	6151.70
14	112.00	15.00	48.80	52.50	67.17	66.17	58.19	6517.14
15	112.00	15.00	52.50	56.20	67.17	66.17	61.21	6855.04
16	112.00	15.00	56.20	59.90	67.17	66.17	63.96	7163.98
17	112.00	15.00	59.90	63.60	67.17	66.17	66.45	7442.65
18	112.00	15.00	63.60	67.30	67.17	66.17	68.66	7689.88
19	112.00	15.00	67.30	71.00	67.17	66.17	70.58	7904.61
20	112.00	15.00	71.00	74.20	67.17	66.17	58.92	6599.01
21	112.00	15.00	74.20	78.00	67.17	66.17	19.67	2202.77

G Funicular polygon method of thrust line analysis

The methodology presented here is reproduced from Miryam Dreyfuss thesis.[8]

The funicular polygon method of thrust line analysis became a standard way of analyzing arches in the nineteenth century when the introduction of graphical methods made it more user-friendly than the mathematical methods with which the principles were developed. I use it in Chapter 8 to test the efficacy of various techniques discussed in this study. In what follows, I provide an example of how to perform a simple thrust line analysis for a barrel vault. It can be done with a pencil and paper, but I use AutoCad for greater accuracy and ease.

PART 1
Steps for construction the thrust line through a barrel vault (Figure G.1):

Step 1: Draw a scaled profile of the vault to be analyzed (shaded area in Drawing 1)
Step 2: Divide the vault into an odd number of vertical sections (the more sections the more accurate the final curve) so that the middle section is centred on the crown of the vault. Number each section starting with "1" at the far left.
Step 3a: Determine the unit weight of the material used for each section kg/m^3. Calculate the mass (M) of each section in m^3 and multiply it times unit weight of the material used. The weight (W) in kg must then be translated into units of force in Newtons (N) by multiplying by 9.8 m/s^2. These are the force vectors, each of which is referred to by the number of its corresponding section, for example F_1, F_2, F_3, and so on.
Step 3b: To draw the force vectors, choose a convenient scale for the vectors so that each unit in the drawing equals a certain number of Newtons (eg., scale above Drawing 2). Draw each calculated force vector as point load located at the centre of gravity of its section. (A program such as AutoCad can calculate the centre of gravity of unsymmetrical shapes automatically.)
Step 4: Out to the side of the drawing of the vault (Drawing 1), draw the force vectors end to end (Drawing 2), one above the other at the same scale as represented on Drawing 1. Then pick an arbitrary point (the trail pole-O') and connect the ends of the vectors labeled a, b, c, and so on, to O' so that you have a series of radiating lines: aO', bO', and so on (the thin solid lines on Drawing 2)
Step 5: Below Drawing 1, project the line of action of each force down to a base line (Drawing 3). Then starting at the left where the line of action of F_1 intersects the baseline at point x', draw a line parallel to line bO' (from Drawing 2) until it intersects the line of action of F_2 (ignore line aO' for now). At this point, draw the next line parallel to line cO' until it intersects the line of action of F_3. Continue until the diagram looks similar to Drawing 3. Then connect points x', y', and z' to form a triangle x'y'z'. These points represent the intersections of the curve just drawn and the lines of action of the middle (F_5) and the two outermost (F_1, F_9) force vectors.
Step 6: Go back to Drawing 2 and draw lines parallel to lines x'y', y'z', and x'z' (represented as single dash-dot lines on both Drawings 2 and 3) so that they pass through the trial pole O'.
Step 7: Return to Drawing 1 and determine the three points (x, y, and z) through which the thrust curve should pass. All three points must be located on the line of action of one of the force vectors. To determine the minimum thrust (i.e. the steepest possible curve that will fit within the arch) for a barrel vault, one point (y) should be at the crown of the extrados. The other two points (x and z) should be on the lines

of action of the outermost (F_1, F_9) force vectors. These locations can be estimated to get an idea of the path of the thrust line and then adjusted later. (In Drawing 1, I chose to start with the intersections at the impost of the vault.) Connect the three points with lines forming a triangle xyz. Ultimately, you want to define the curve that is tangent to the arch in three point. These are the three "hinges" of the three-hinge arch explained in Chapeter 8.

Step 8: Go to Drawing 2 and draw lines parallel to lines xy, yz, and xz from Drawing 1(dotted lines) such that they pass through the intersections of the vertical lines of vectors (a_j) and the lines x'y', x'z', and y'z'. The intersection of the lines xy, yz, and xz provide the pole point O. The horizontal distance from O to the vertical line of vectors (a_j) represents the horizontal thrust acting on the arch or vault.

Step 9: On Drawing 2, draw lines connecting the pole of point O to the ends of the vectors creating lines aO, bO, cO, and so on (thick dash-double dot lines).

Step 10: The final step is to plot the final line of thrust for the vault. On Drawing 3, draw a line parallel to line aO from Drawing 2 starting at point x' (draw down and to the left). This is the vector representing the thrust on the abutment. Go back to point x' and draw a line parallel to line bO from Drawing 2 until it intersects the line of action F_2. Then draw a line parallel to line cO until it intersects the line of action of F_3. This process is a repeat of that in Step 5. The curve (thrust line 1) can then be transferred to Drawing 1 to see how it related to the vault. (The curve can actually be drawn directly onto Drawing 1, but it is easier to see on Drawing 2.) If the final curve is tangiest to the intrados of the arch, points x and z must be mode up or down along their respective lines of actin. Moving the points up will spread the curve out making it less steep, and moving them down will bring the curve in making it steeper. In the example illustrated, the cure needs to come in to touch the intrados, so the points are moved down. Connect the new points, r and s, so that they form triangle rys. then repeat steps 8-10 as shown in Drawing 4 to create thrust lines 2. Once the curve is tangent to the vault in three points, it is at the state of minimum thrust, which is the limit state indicating the point of stability because of the three hinges. This is a trial and error process and may take more than one try!

PART 2

Plotting the line of thrust from the vault down through the abutment: In the previous section, the minimum thrust of a stable three-hinged arch was established. The final part of determining the stability of the structure is to see whether the line of thrust remains within the thickness of the abutment. Because the drawing is symmetrical, the instructions are given only for the left abutment.

Step 1: Calculate the mass (M_b) of the abutment and multiply it times the unit weight of the material used. Translate this weight into a force (F_b) into Newtons by multiplying it by 9.8 m/s^2.

Step 2: Determine the centre of gravity of the abutment. For a rectangular abutment of the same material throughout, it will be located on the vertical centerline. This is the line of action of the force F_b.

Step 3: At the intersection of line rn and the line of action of F_b, mark point t. Using the same scale used for the thrust line of the vault, draw a vector equal to F_b from t straight down along the line of action to k, such that tk = F_b. At point k, draw a line parallel and equal in length to line rn to create line ka. Finally, draw a line from t to a. This vector ta represents the magnetite and direction of the thrust on the abutment. If the line of action of vector ta remains within the thickness of the abutment, the structure is in equilibrium and will stand; however, a margin of safety is always desirable.

The process just described provides the steps involved in creating a funicular polygon diagram, but it does not explain the reasoning behind these steps. For further explanation of the funicular polygon methods, see W. Zalewski and E. Allen, *Shaping Structure* (1998).

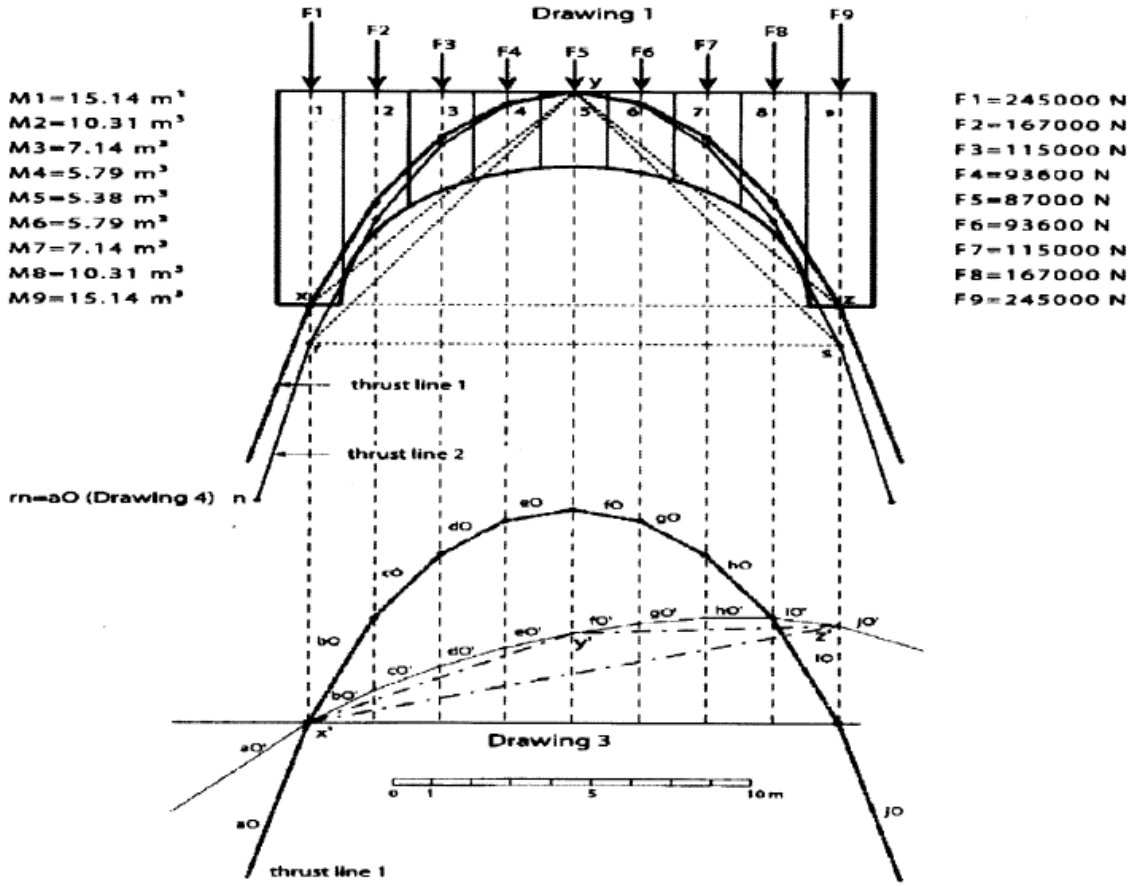

Figure G.1: Drawings 1 and 3 of the funicular polygon method of thrust line analysis [8]

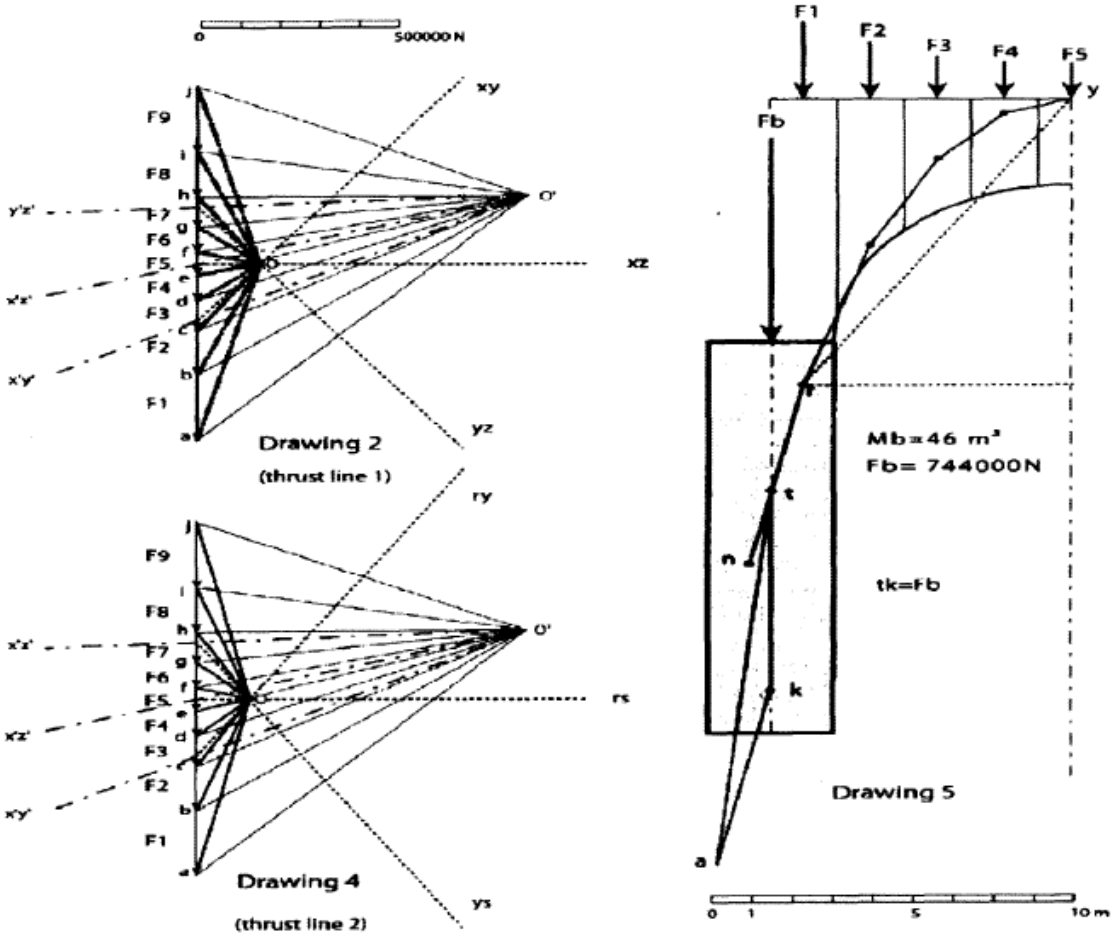

Figure G.2: Drawings 2,4, and 5 of the funicular polygon method of thrust line analysis [8]